sustainability

MDPI

Review

Recent Advances in Flexible Solar Cells; Materials, Fabrication, and Commercialization

Maoz Maoz [1,*], Zohair Abbas [2], Syed Abdul Basit Shah [1] and Vanni Lughi [1]

[1] Department of Engineering and Architecture, University of Trieste, Via Valerio 6/A, 34127 Trieste, Italy; syedabdulbasit.shah@phd.units.it (S.A.B.S.); vanni.lughi@dia.units.it (V.L.)
[2] Electronics Engineering Department, University of Rome Tor Vergata, Via del Politecnico, 00133 Rome, Italy; zohair.abbas@uniroma2.it
* Correspondence: mmaoz@unisa.it

Abstract: Flexibility, light weight, and mechanical robustness are the key advantages of flexible photovoltaic (PV) modules, making them highly versatile for sustainable energy solutions. Unlike traditional rigid PV modules, their flexible nature makes them incredibly versatile for harnessing energy in places where doing so was once impossible. They have a wide range of applications due to their flexibility and moldability, making it possible to conform these modules to surfaces like curved rooftops and other irregular structures. In this paper, we provide a comprehensive review of all the materials used in flexible PV modules with a focus on their role in sustainability. We thoroughly discuss the active-layer materials for crystalline silicon (c-Si)-based solar cells (SC) and thin-film solar cells such as cadmium telluride (CdTe), as well as copper indium gallium diselenide (CIGS), amorphous thin-film silicon (a-Si), perovskite and organic solar cells. Various properties, such as the optical, barrier, thermal, and mechanical properties of different substrate materials, are reviewed. Transport layers and conductive electrode materials are discussed with a focus on emerging trends and contributions to sustainable PV technology. Various fabrication techniques involved in making flexible PV modules, along with advantages, disadvantages, and future trends, are highlighted in the paper. The commercialization of flexible PV is also discussed, which is a crucial milestone in advancing and adapting new technologies in the PV industry with a focus on contributing toward sustainability.

Keywords: flexible solar cells; absorber layer; substrate materials; fabrication; thin film; electrodes; polymers; efficiency

Academic Editor: Cinzia Buratti

Received: 31 December 2024
Revised: 5 February 2025
Accepted: 6 February 2025
Published: 21 February 2025

Citation: Maoz, M.; Abbas, Z.; Shah, S.A.B.; Lughi, V. Recent Advances in Flexible Solar Cells; Materials, Fabrication, and Commercialization. *Sustainability* **2025**, *17*, 1820. https://doi.org/10.3390/su17051820

1. Introduction

The rising growth in the utilization of solar photovoltaics (PVs) and the provision of energy for the planet's rapidly growing population has shifted the interest of research and development (R&D) institutions, public policymakers, and investors in PVs. The per-watt price of PVs has dropped since their initial introduction to the market from 100 USD to 3 USD. Currently, 51% of solar PV capacity is provided by utility-scale plants, followed by residential and commercial segments, which account for 28% and 19%, respectively. Silicon (Si) dominates the PV market with a market share of around 95%. This accelerated further in 2021 with a shift towards more efficient mono-crystalline wafers in almost all PV crystalline production. Currently, new, even more efficient cell designs like TOP-Con, heterojunction, and back-contact technologies have seen a promising increase in commercial production and accounted for 20% of the market [1].

Thin-film technology was first used for powering wristwatches and calculators in the late 1970s. A significant rise in the advancement and development of thin-film solar technologies has been observed in the last two decades. These PV technologies are made up of a diverse range of semiconductors involving organic and inorganic materials and, more recently, hybrid semiconductor materials. Furthermore, secondary materials that enhance the functionality of these cells, such as those resulting from solution engineering, are the driving factors for these technologies. In contrast to conventional PV technologies based on crystalline silicon (c-Si) solar cells (SCs), thin-film technologies rely on complex physical phenomena like the charge-separation mechanism, exciton operation, and functionality of interface layers. In the early life of thin-film technologies, research was focused on understanding the operational mechanisms and power-conversion efficiency. However, recently, as the technology has advanced, more focus has been placed on understanding degradation phenomena to improve overall device stability. To commercialize these technologies, it is essential to improve the power-conversion efficiency as well as the lifetime stability of these devices [2].

Traditional c-Si PV modules are heavier than flexible thin-film solar modules. Moreover, these thin-film-based modules may easily be bent and molded into various shapes based on the requirements of the product or application. Flexible solar modules are extremely demanding energy solutions for commercial products, where the specific power, total weight, and mechanical impact strength are crucial [3]. One such example is the integration of semi-flexible solar panels into the roofs of boats as a secondary source of charging. Flexible modules have also been promoted as building-integrated photovoltaic (BIPV) cells to increase the self-sufficiency of buildings, as shown in Figure 1.

Figure 1. Flexible roof-top photovoltaic cells.

Similarly, the use of lightweight flexible PV modules for powering electronic gadgets is rapidly growing. With this rapid progress in research and development and the growing commercialization of these new materials, i.e., systems like organic and inorganic semiconductors and hybrid semiconductors, both semi-flexible and flexible PV modules are expected to have a major market share in the near future. The current revenue share of thin films exceeds 25% of the total PV market. The global flexible solar-panel market size is expected to double by 2030, reaching a value of USD 914 million from 2021 to 2030 [4]. The growing interest in flexible PV technologies has recently attracted the interest of researchers, policymakers, industrial experts, and innovators.

This study aims to fill a gap in the literature by compiling the existing literature that addresses the specific technology of photovoltaics, involving current trends and advances in flexible solar cells in a single paper. The topics that are addressed in this paper include materials for active layers, substrate, and electrodes, discussion on essential properties for

flexible solar cells/modules, fabrication techniques, commercialization, and application. This review paper, in addition to the introduction, also has a section on the organization of the article, flexible photovoltaic materials, and, later on, a section on commercialization. The articles conclude with final deliberations regarding this topic.

2. Research Method

This research is based on a systematic literature review. It is initiated by defining the research problem, which is how flexible photovoltaic cells/modules have been approached in scientific literature published up to 2023. After the definition of the problem, the second stage is to formulate the search strategy. The University of Trieste (access through institution) approach is used to access research databases like Web of Science, Scopus, and Google Scholar. The keywords used for the search are flexible photovoltaic, flexible solar cells, flexible substrates, flexible thin film, flexible crystalline silicon, flexible organic sells, flexible electrodes, and flexible photovoltaic market. The third phase involves the selection of relevant papers based on the keywords. The search was not limited by the years of publication. In the fourth phase, articles were thoroughly read, and necessary findings were extracted and added to the predefined sections. In the last phase, the study was organized and summarized to give coherent, comprehensive, and complete findings on the research problem.

3. Flexible Solar Cells/Modules (Materials)

The common structure of flexible solar cells is shown in Figure 2. The cell can be developed on both opaque and transparent substrates depending upon cell architecture requirements. Generally, for thin-film solar cells, various functional layers are deposited on the flexible substrate using different deposition techniques such as spin coating, inkjet printing, high-temperature and low-temperature chemical vapor deposition, vapor-phase deposition, and sputtering [5].

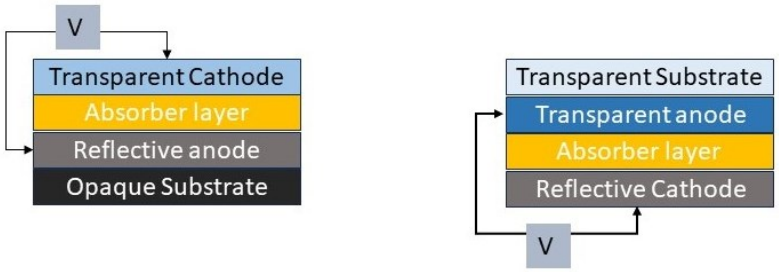

Figure 2. Schematics of possible cell architecture.

The substrate protects the cell from environmental degradation and provides mechanical support while simultaneously allowing flexibility to curve and bend. The electrodes not only collect photogenerated charge carriers but also act as electrical conductors to the external circuit. One of the electrodes must be optically transparent so the sunlight can reach the active-layer material and create photoinduced charge carriers [6]. The key component of flexible solar cells is the active-material layer that plays a critical role in the power-conversion efficiency of the device [7]. The common active materials for flexible solar cells are of three types: organic semiconductors [8], inorganic semiconductors [9], and hybrid semiconductors with both organic and inorganic materials [10]. Common inorganic semiconductors for flexible and semi-flexible solar cells are crystalline silicon [11], amorphous silicon, CdTe, CIGS [12]. Organic semiconductors for flexible solar cells include donor and acceptor compounds, which include polymers like P3HT (poly(3-hexylthiophene), PTB7 (Poly[4,8-bis(5-(2-ethylhexyl)thiophen-2-yl)benzo[1,2-b;4,5-b′]dithiophene-2,6-diyl-

alt-(4-(2-ethylhexyl)-3-fluorothieno[3,4-b]thiophene-)-2-carboxylate-2-6-diyl]), and others, including PCBM (Phenyl-C61-butyric acid methyl ester), DPP (Diketopyrrolopyrrolo) and IT-4F (3,9-bis(2-methylene-((3-(1,1-dicyanomethylene)-6,7-difluoro)-indanone))-5,5,11,11-tetrakis(4-hexylphenyl)-dithieno[2,3-d:2′,3′-d′]-s-indaceno[1,2-b:5,6-b′]dithiophene) [13]. Hybrid organic/inorganic flexible solar cells are mostly comprised of metal halide perovskites as an absorber layer or active layer [10]. The highest reported single-junction solar-cell power-conversion efficiency for different active-layer materials used for both traditional and flexible PV is given in Figure 3 [14].

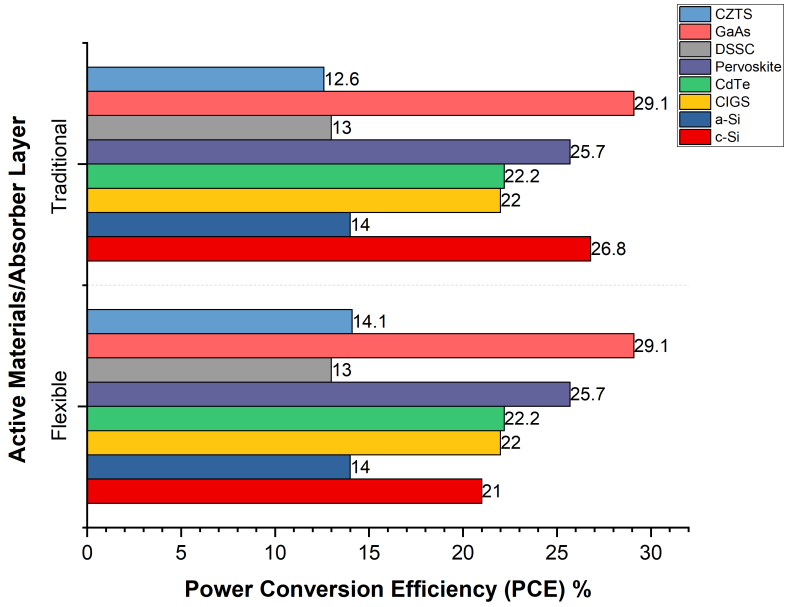

Figure 3. Comparison of power-conversion efficiency for different active-layer materials for traditional and flexible PV.

3.1. Active Materials

This section focuses on discussing active materials that have been used in the past for flexible solar cells. In this article, the term "active material" refers to the "light-absorber layer". For flexible solar cells, the preferred processing temperature is usually less than 300 °C due to the limitations of the common polymeric substrate used. However, for willow flexible glass and metallic substrates, this temperature can go higher [15]. Similarly, the active-material thickness ranges from a few microns in the case of silicon, CIGS, and CdTe to a few nanometers in the case of organic PV and other thin-film technologies. To improve the conversion efficiency, flexible active materials with a broad absorption spectrum are desirable [16]. Flexible solar cells require photoactive materials that can withstand repeated bending and stretching without significant degradation in performance. Materials with high mechanical flexibility and stability are essential [17]. For flexible solar commercialization, the fabrication should be scalable and cost-effective. Materials with abundant and low-cost resources are desirable for commercial viability. This section discusses the fundamentals of these active-layer materials with particular emphasis on their strengths, weaknesses, and prospects. The brief summary of this section is given in Table 1.

Table 1. Advantages and disadvantages of active materials used for flexible PV.

Technique	Advantages	Disadvantages
c-Si	Limited Flexibility Higher temperature processing Thickness 50–150 µm	Abundant Resources Higher Efficiency 26% in Band gap 1.1 eV
a-Si	Higher Band Gap 1.7 eV Light-Induced Degradation (Steabler–Wornski Effect) Lower efficiency 14%	Good flexibility Higher mobility Can be made thinner up to 1 µm Can be used for indoor applications
CdTe	Toxicity Recycling issues Lower flexibility compared to organic solar cells	Higher efficiency 22% Higher Absorption Coefficient Can be made thinner up to a few microns
CIGS	Costly due to the high price of indium and gallium Complex fabrication process	Higher efficiency 22% Tunable bandgap 1–1.7 eV Thickness 5 µm
Pervoskite	Stability issues Prone to moisture, oxygen and UV	Higher efficiency Tunable bandgap 1.5 to 2.4 Thickness 300–500 nm
Organic solar cells	Lower efficiency 13% Stability issue under UV Lower operational life up to 5 years	Printable and flexible Low cost Tunable bandgap Thickness 100–500 nm

3.1.1. Crystalline Silicon (c-Si)

Silicon-based solar cells have the largest PV market share with continuous advancement and widespread applications in our daily lives. Their dominance in the PV market is attributed to its abundance of silicon resources and the technological maturity achieved through decades of research and development. For its excellent operating situations like power-conversion efficiency [18], reliability, durability [19], and safety, it has the potential to explore the avenue of flexible solar modules applications more specifically in buildings, transportation carriers, and electronic devices [20].

Thin c-Si solar cells have higher power-conversion efficiency (PCE) than their non-crystalline counterparts because of their superior electrical and optical performance. However, the thin c-Si flexible solar cells have lower PCE than conventional c-Si solar cells because of serious incident-light management problems [21]. The light management can be improved by employing certain strategies like mitigating refractive-index mismatch between air and c-Si using surface coatings [22]. Similarly, light management can be enhanced by increasing the angle of incidence of light entering the c-Si using the light-scattering mechanism of the surface layer. These surface layers can also be used to improve the optical length, hence enhancing light absorption at higher wavelengths in the near-IR region [23]. Moreover, using adhesion films on the surface enhances surface mechanical stability by managing overall stress distribution on the surface [24]. In addition, the cells can be self-cleaned due to the hydrophobic properties of the films [25]. In the early 1980s, thin-film c-Si was first utilized in cells with highly efficient thin-film fabrication technology [26]. A thin-film solar cell with PCE higher than 4% was developed in 1994 [27]. The efficiency of the laboratory cell increased up to 7% by preventing oxygen contamination in the intrinsic c-Si:H layer. The layer thickness must be kept up to 2 µm to increase the absorption [28]. In 2006, Mia et al. developed thin-film c-Si solar cells that, for the first time, passed the PCE of 10% [29]. The intrinsic layer was deposited using the hot-wire chemical vapor deposition (CVD) technique, which exhibits a better fill factor (FF) and open-circuit voltage (Voc) than the one prepared by plasma-enhanced chemical vapor deposition (PECVD). In 2014, using a textured honeycomb structure, a single-junction thin-film c-Si:H solar cell was fabricated, which achieved PCE of 11% [30]. Later, in 2018, an efficiency increase of up to 12% was further obtained using the same honeycomb textured structure by increasing the deposition rate by up to 1 nm/s and keeping the intrinsic c-Si:H layer at around 2 µm [31]. Similarly, freestanding c-Si is developed using photolithography with an inverted pyramid nanostructure. The flexible freestanding design has shown PCE of 12.3% with a thickness of wafer less than 3 mm [32].

The c-Si can be fabricated by the transfer process. This process was first reported by Werner et al. by transferring the c-Si film to plastic foil. The device achieved a PCE of 14.0% with a thickness of 40 µm. Similarly, using plastic foil, the flexible c-Si was fabricated by transfer process with a thickness of 25 µm. The film can be bent to a curvature of 2 mm with PCE reaching 14.6% [33]. Reuter et al. used porous silicon as a sacrificial layer for transfer printing with a process called epitaxial layer transfer. Freestanding c-Si thin-film solar cells with a thickness of 47 µm achieved PCE of around 17% [34]. The PCE was further improved, reaching 18% by optimizing the process [35]. Bulk wafer etching is another common technique to fabricate ultrathin silicon solar cells. Flexible PV modules with thicknesses between 15 to 20 µm achieve efficiency of up to 8% using bulk wafer etching. Wafer thickness is controlled by etching time. The fabricated modules retained their efficiency over 200 bending cycles with a bending radius of 5 mm [36]. A flexible thin-film module based on hexagonal Si segments was fabricated using an etching method with PCE approaching 15% [37]. Similarly, 45 µm flexible solar cells were developed using Cu-assisted chemical etching with PCE of 17.3% [38]. Another promising technique to fabricate ultrathin crystalline silicon solar cells is exfoliation, because of the simplicity of the cleaving process. Using the exfoliation method with aluminum as a metallization layer, a 25 µm c-Si thin film is fabricated with cell PCE of 12.5% [39]. A kerf-less exfoliation method in which a thin layer is exfoliated from a thicker parent wafer by thermal process is used to prepare thin-film c-Si solar cells with a thickness of approximately 25 µm. The cell is based on an unoptimized single heterojunction design, achieving an efficiency of 14.9% [40].

For flexible crystalline silicon solar cells, the light absorption is strongly influenced by the thickness of the substrate. The flexibility of the wafer is also directly related to the flexibility, i.e., the bending radius as given by Equation (1) [41].

$$R = E(T/2)\sigma_{st} \quad (1)$$

where R is the bending radius, T is the thickness, σ_{st} indicates bending stress, and E is Young's Modulus. As indicated in the equation, the mechanical flexibility increases with reducing thickness. However, the optical performance deteriorates due to the Lambertian limit. This is the thermodynamics limit required to attain maximum absorption for a given thickness of material. To reach this limit, the flat surface is altered to diffuse light and increase the optical path length. To reach the Lambertian limit of light absorption, different light-trapping strategies are employed [42] such as pyramids, gratings, non-periodic textures, and plasmonic effects [43]. Both random [44] and periodic pyramid [45] textures are used to improve light-trapping. Random pyramid and periodic pyramid textures were compared with each other in ultrathin crystalline silicon solar cells. The random pyramid textures show better light-trapping for shorter wavelengths of light due to nanopyramids. However, the periodic pyramid texture shows better light-trapping for longer wavelengths due to shorter wavelength interference and longer optical length [46]. Grating or photonic crystals are used to improve the light-trapping in the ultrathin c-Si. These are periodic arrangements of dielectric or metallic materials at the scale of the wavelength of light, which allow only specific wavelengths to propagate. These are integrated into the active layer of thin-film solar cells, which increases the light absorption for a wider range of wavelengths and different angles of incidence. These photonic crystals improve the short circuit for the incident light by 47% [47]. In another study, light management is improved through the optimization of c-Si microwire size and spacing. These microwire-based c-Si thin-film solar cells have achieved a PCE of 18.9%. These cells retained efficiency even after 1000 bending cycles [11].

3.1.2. Amorphous Silicon (a-Si)

Amorphous silicon (a-Si) solar cells are one of the best counterparts to the c-Si because of their low-cost manufacturing. They are best suited for large-scale PV module manufacturing due to their low material cost [48]. Due to inherent disorders in the a-Si active layer, it has a higher absorption coefficient. This property of a-Si can reduce the thickness of the material up to 500 nm, hence reducing the cost further [49]. However, the presence of inherent disorder in the structure leads to incomplete bonds called dangling bonds. These defect sites or incomplete bonds also act as recombination points, which reduce the photoconductivity of the film [50]. Plasma enhances chemical vapor deposition, and sputtering is usually used for thin-film a-Si deposition. These processes provide better control of electrical and structural properties, resulting in high-quality films [51]. E-beam deposition is also used for a-Si thin-film deposition [52]. a-Si has a high defect density, which causes charge-carrier recombination, hence reducing its suitability for photovoltaics. This problem can be reduced by the hydrogenation of a-Si represented as a-Si:H. However, prolonged exposure to sunlight degrades the performance of the a-Si:H, which is called the Staebler–Wronski effect [53]. Light-induced defect creation can be observed in the hydrogenated a-Si:H. The light generates an electron–hole pair, which recombines in a localized state associated with defect states already present in the disordered structure of amorphous silicon [54]. To minimize this effect, the thickness of the film is reduced, but it can cause a reduction in the PCE of the cell. The increase in the growth rate of the intrinsic layer deteriorates the performance. The chemical stability of the solar cells improves by increasing the deposition temperature; however, it causes low open-circuit voltage (Voc) and short-circuit current (Isc) [55].

Superstrate (p-i-n) and substrate (n-i-p) as shown in Figure 4 are the two configurations in which a-Si:H SC was often manufactured. In the (p-i-n) configuration, the substrate must be both temperature-resistant and transparent, but in the (n-i-p) configuration, the substrate is flexible and opaque, such as in polymers and stainless steel [56]. As a-Si:H SC has a high photo-to-dark conductivity ratio, there is less efficiency loss when there is less illumination. Therefore, a-Si SC is employed for indoor and low-light applications. Many electronic circuits need a minimum voltage of roughly 0.5 V, which a-Si:H can deliver under extremely low illumination conditions [57]. When exposed to the outdoor environment, the a-Si modules start their degradation in the early days of exposure and continue to degrade over time. This is an unwanted condition for the performance and reliability of the modules. With every 1 °C rise in temperature, the a-Si solar-cell power is reduced by 0.2%, which is less than the c-Si PV modules [58].

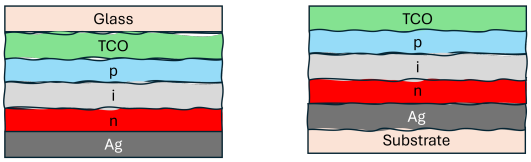

Figure 4. p-i-n (superstrate) and n-i-p (substrate) a-Si:H cell structure.

The optical performance of a-Si:H can be improved by employing an a-SiN:H layer acting as a refractive-index-matching and anti-reflection coating layer between the conductive oxide and glass. These coatings aim to reduce front-side optical reflection and provide surface passivation. This layer addresses the refractive-index mismatch between the conductive oxide and the glass substrate by tuning the refractive index and thickness. The PE-CVD technique is used to fabricate this layer. By varying depiction conditions, different refractive-index layers can be obtained [59]. The use of titanium dioxide (TiO) nano-patterns improves the performance of a-SiN:H. It increases chemical stability and

improves the transmittance. The higher refractive index of these layers acts as an anti-reflection (AR) layer. Using the TiO layer, a PCE of 6.4% was achieved [60]. High vapor pressure treatment of the a-Si:H solar cells increases its PCE to 8.4% due to the reduction in charge recombination [61]. The impact of carrier trapping is a crucial factor in restricting carrier transport and hence improves the performance of a-Si:H solar cells. To improve their electrical performance, it is essential that the Urbach energy (total energetic disorder of the system usually governed by structural disorder and imperfections) should be reduced to below 45 meV and the charge-carrier density to below 10^5 [62]. The use of plane and textured transparent conductive oxide layers (TCO) increases the efficiency of a-Si:H solar cells. The ZnO textured reported a PCE of 18.6%, whereas textured indium tin oxide (ITO) reported a PCE of 16.3%. The ZnO TCO is better than ITO TCO in terms of both cost and efficiency [63].

3.1.3. Cu-Based Solar Cells

Cu-based thin-film solar-cell materials are considered environmentally friendlier than CdTe and Si-based solar cells. They are chemically stable and have a decent PCE of around 19% on module level [64]. They can be fabricated using various techniques, which include solution processing and vacuum deposition ranging from low to high temperature [65]. This gives freedom to deposit these thin films on various substrates. It has a wider range of applications in optoelectronics, which operates in a wider wavelength range due to easily tunable bandgaps [66]. In the case of solar cells, Cu thin-film technology can be used as a photoactive material layer or contact layer. These films are mostly used as photoactive material layers because of their higher hole mobility, higher absorption coefficient, chemical stability, and tunable bandgaps. The most widely used Cu-based thin-film technologies are ternary Cu chalcogenides such as CIS (copper/indium/sulfur/selenium2), quaternary Cu chalcogenides such as CIGS (copper/indium/gallium sulfur/selenium4) and kesterite such as CZTS (copper/zinc/tin sulfur/selenium4). The bandgaps for these materials are low, ranging from 1.0 to 1.2 eV [67].

CIS-based thin-film solar cells have more potential to absorb a wider range of solar wavelengths and act as one of the most suitable materials for photoactive layers in solar cells [68]. However, its PCE has not crossed 19% due to impurity issues in its thin-film development. The higher concentration of impurities is due to Cu vacancies or antisites. This lowers the charge-transport properties and hence reduces the PCE [12]. The theoretical limit of 95.7% of the Shockley–Queisser (SQ) limit was achieved with a current density of 42.3 mA/cm^2 with a bandgap of around 1 eV. The limiting Voc and FF further reduces the PCE, which corresponds to around 70% of the SQ theoretical limit of the single-junction solar cell of CIS, which is 30.8% [69]. The crystal quality and morphology control improve the PCE of the CIS [70]. The uniform morphology, larger grain size, and denser surface enhance the PCE. This can improve the PCE by up to 9%. The improved surface density and microstructure of the CIS could improve the charge recombination and hence improve Voc and FF [71]. For the development of CIGS, CIS compounds are used as starting materials by partially replacing indium with gallium in the compound. The resultant CIGS have higher bandgaps than CIS compounds. The bandgap depends upon indium and gallium content [72]. The bandgap for CIGS is around 1.10 eV, therefore acting as a perfect material for a photoactive layer. The bandgap grading is used to optimize the performance of the CIGS solar cells. The increase in the ratio of gallium replacement with indium increases the bandgap of the CIGS materials, reaching up to 1.70 eV. CIGS-based solar cells have shown a PCE of around 23%. CIGS-based solar cells that give higher PCE are cadmium (Cd)-free buffer layers [73]. These cadmium sulfide (CdS) buffer layers are replaced with zinc sulfide (ZnS) n-type buffer layers, which have better optical and electrical properties. To improve

the cell performance of CIGS, different strategies have been developed and applied. The highest confirmed PCE of 23.35% is shown using a zinc-based double buffer layer in place of the CdS layer [74].

The reaction between ternary copper (Cu)-chalcogenides and ZnS or Zinc selenide (ZnSe) compounds gives rise to kesterite CZTS [75]. Its bandgap ranges between 1.04 and 1.50 eV. It intrinsically has p-type characteristics and exists in two different crystal structures, namely stannite and kesterite. The latter is more stable, with an excellent absorption coefficient [76]. Kesterite CZTS have moderate PCE of around 12%. The reason for lower PCE is Voc losses due to non-radiative recombination caused by defects in the bulk and film surface. The grain size and degree of crystallinity affect the PCE. Higher grain sizes and uniformity in the morphology of the film result in lower charge recombination and hence improve the PCE of CZTS [77]. The better smooth surface morphology of CZTS reduces recombination at the interface between the layers. The degree of crystallinity helps in restricting secondary phase formation of the photoactive layer [78].

3.1.4. Cadmium Telluride CdTe

CdTe solar cells have shown promising scalability among thin-film technologies. They are considered one of the promising technologies that can be easily used as thin films in PV modules because of their near-optimal bandgap, which ranges between 1.39 and 1.5 eV, higher absorption coefficient, and chemical stability [79]. Another important aspect of CdTe solar cells is that they can withstand high temperatures and radiation [80]. CdTe solar cells have shown efficiency up to 22% in superstrate configuration [14]. Usually, the CdTe thin-film solar cells are produced in a superstrate configuration. In superstrate configuration, performance is improved by carrying out a process called activation treatment. In activation treatment, the Cd-chloride layer is deposited on top of the film and then air-annealed. This treatment helps improve the electrical properties of the thin film [81]. CdCl treatment helps in the recrystallization and grain growth of CdTe thin film. Also, it helps reduce the lattice mismatch between the CdT and CdS layer as the sulfur diffuses into the CdTe thin film between the layers [82]. However, higher chlorine treatment and higher deposition temperature results in inconsistent microstructures [83].

In substrate conditions, Cu is required to be added as back contacts. The Cu is added as a back contact during the deposition of CdTe. This deposition results in a reaction between the Cu and CdTe film, which causes cell degradation [84]. This degradation phenomenon can be decreased by either using the Cu-free back contacts or by controlling the Cu diffusion by controlling the annealing time and temperature. Usually, the Cu diffusion takes place at around 400 °C. CdTe has been further improved by replacing the CdS layer with a transparent buffer layer of oxides such as magnesium zinc oxide [85]. The removal of CdS, which has a higher bandgap and melting point, helps reduce parasitic absorption at shorter wavelengths. It also helps improve the lifetime of photocarriers. Also, bandgap grading helps improve the overall efficiency of CdTe thin films [86]. The quantum efficiency of CdTe in recent devices has been improved by introducing $CdTe_{1-x}Se_x$ alloy in the absorber layer, therefore achieving a bandgap of 1.39 eV, which is lower than the pure CdTe film [87]. This helps increase the photocurrent in the absorber layer of CdTe film. Also, the Se inclusion enhances the lifetime of the grains. Although the bandgap is decreased, it maintains Voc. The content of Se is between 20% and 40% in current cells [88].

Another important aspect is improving power-conversion efficiency by doping with Group V elements (P, As, and Sb). This helps increase hole concentration and open-circuit voltage. In one study, polycrystalline CdTe was doped with As. This treatment increased the majority carrier density by a magnitude of 1016 cm^3. It also helps greater photocurrent generation with improved stability, achieving PCE of 20.8% [89]. In another similar study,

the comparison of doping of Group V elements (P, As, and Sb) was carried out. It was observed that Sb is a more attractive dopant than P and As because of its longer stability and better lifetime [90]. Phosphorous (P), arsenic (As), and antimony (Sb) act as shallow acceptors, showing decreased ionization energies when doped with CdTe thin-film solar cells. These shallow acceptors are unstable and behave like hydrogenic impurities. They do not limit p-type doping and hence result in better cell efficiency [91].

3.1.5. Perovskites

Perovskite-based solar cells are considered one of the most promising technologies because of their higher power-conversion efficiency, ease of fabrication at lower and semi-lower temperatures, and low cost due to cheaper materials. Flexible perovskites are bendable and lightweight and can easily be transported and installed on curved surfaces like buildings, portable electronics, space applications, and other energy systems [92]. Metal halide perovskites have outstanding optoelectronic properties as they form a direct bandgap. They can be fabricated at lower temperatures. Typical metal halide perovskites have a 3D crystal structure represented by the general formula ABX_3. In the ABX_3 crystal structure, A represents the monovalent cation, usually formamidinium (FA^+), methylammonium (MA^+), and cesium (Cs^+), B represents divalent metal cations, usually lead (Pb^{+2}) and tin (Sn^{+2}), and X represents the halogen anion, mostly iodine (I), bromine (Br) or chlorine (Cl) [93]. Octahedral factor (v) and Goldsmith tolerance factor (t), which depend on the ionic radii of A, B, and X, govern the crystallographic stability and structure of the perovskites. When the t and v are in the range of 0.81–1.11 and 0.44–0.90, respectively, they form a 3D crystal structure. However, if the radius of the cations exceeds the Goldsmith tolerance factor, it forms the 2D or quasi 2D perovskites called the Ruddlesden–Popper phase [94].

The very first flexible perovskite solar cells (FPSC) achieved a PCE of around 2.6% on a polymer substrate developed in 2013 [95]. To improve the PCE of flexible perovskite solar cells, many efforts have been made since then. Some structural design changes and new material development have improved the mechanical stability and PCE of FPSCs. A low-temperature solution-based organometal trihalide perovskite $CH_3NH_3PbI_{3-x}Cl_x$ was developed on polyethylene terephthalate (PET) polymer with PCE reported to be around 6% [93]. In another effort, using ZnO nanoparticles as electron transport layers (ETLs), $CH_3NH_3PbI_3$-based solar cells as a perovskite absorber layer achieved PCE of around 10% [96]. A dimethyl sulfide (DS) additive was used to improve the performance of FPSCs as the DS additive reacts with Pb^{+2}, resulting in the formation of a chelated intermediate. This significantly reduces the crystallization rate, which results in large grain size and good crystallinity for the resultant perovskite film. The PCE of the flexible perovskite solar cells increases to 18.40% [97]. A PCE of more than 19% was achieved in flexible planar FPSCs using ligand and additive synergetic processes. Due to the synergetic effect of the additive CH_3NH_3Cl, FA-based perovskite film is developed on the flexible substrate, which showed a large grain size and high crystallinity under ambient conditions [98]. The efficiency was further improved to 21% by passivating the mixed-cation perovskite film with artemisinin. This decreases the trap density and hence effectively reduces non-radiative recombination losses [99]. A multifunctional agent, histamin diiodate, is used between the SnO/Perovskite interface, which helps in surface charge extraction and improves the charge transport between the layers. This additive developed as a low-process solution acting as an ETL in FPSC, which has achieved an efficiency of 22.44. Recently, a stable inverted FPSC was developed with interfacial modification through a pentyl ammonium acetate (PenAAc) molecule between the hole-transport layer (HTL) and perovskite film. The cell achieved a record PCE of 23.68% [100].

Recently, rapid progress has been achieved in terms of the PCE of FPSCs; however, there are still significant factors impeding the improvement of FPSCs. The morphology of functional layers, more specifically the perovskite absorber layer, plays a crucial role in the performance of FPSCs. The morphologies of perovskite absorbers in FPSCs are difficult to manage due to the fabrication complexity of the flexible and soft substrate [101]. Due to the limitation of the temperature and thermal conductivities of the flexible substrate, it is difficult to fabricate a high-quality perovskite layer. This results in lower values, open-circuit voltage charge density, and fill factor. Also, the flexible substrate for FPSCs has lower optical properties in contrast to its rigid counterparts [102]. FPSCs mostly exist in mesoporous or planar structures. Mesoporous FPSCs are usually based on mesoporous TiO_2, which is present at the bottom of the absorber layer and helps in establishing good contact between ETL and the absorber layer. This is very beneficial for electron extraction. However, fabrication of TiO_2 requires a higher temperature that limits its use for FPSCs [103]. Planar structure can be further broken down into two configurations, usually depending upon the arrangement of electron and hole-transport layers. The two configurations are regular planar (n-i-p) and inverted planar (p-i-n) [104]. The planar structure is simpler than the mesoporous structure as it does not have the scaffold layer [105]. This helps in developing thin-film structures at low processing temperatures. In planar structure, the perovskite absorber layer is sandwiched between the HTL and ETL [106]. The difference between the inverted and regular structure is the deposition of ETL and HTL. Inverted FPSC configuration shows a greater advantage over its regular counterpart with higher reliability, less hysteresis, and more potential for making tandems [107].

The most fundamental absorber layer that was first utilized as a perovskite structure in solar cells is $MAPbI_3$. However, it faces chemical and thermal stability issues when exposed to a real environment, as compared to other solar technologies. To cope with these issues, another perovskite material, $FAPbI_3$, was later used because of better thermal stability and narrower band gap as compared to $MAPbI_3$. However, $FAPbI_3$ also requires a higher temperature (150 °C) for post-heat treatment due to the presence of a yellow phase (which exists at 100 °C), which impedes its application on plastic substrate [108]. To favor the fabrication process and improve the performance of the perovskite absorber layer, a mixed-cation system was introduced. Initially, MA+ was introduced in $FAPbI_3$ material. This not only lowers the annealing temperature but also results in the suppression of the yellow phase in the $FAPbI_3$ system [109]. To further improve the performance of the absorber layer, a mixed anion in the form of Br- was also introduced [110]. $(FAPbI_3)_{0.85}(MAPbI_3)_{0.15}$, a combination of mixed cation and anion was used, which not only enhances the crystallinity but also eliminates the yellow phase [111]. After the optimization of the combination of $(FAPbI_3)_{0.85}(MAPbI_3)_{0.15}$, the cesium was introduced in the mixed cation and anion system, which helps improve the thermal stability of the layer. The introduction of multiple cations further enhances the PCE, also improving bendability, which is an essential requirement for flexible solar cells [112]. A record efficiency of 19.11% was demonstrated with a quintuple-cation system-based perovskite absorber layer $Rb_{5-x}K_xCs_{0.05}FA_{0.83}MA_{0.17}PbI_xBr_{3-x}$. This combination has retained 93% of its PCE after 2000 bending cycles and 68% of PCE after 1000 h in an 85 ºC nitrogen environment [113].

Another important aspect of FPSC is its performance in the bending state at different angles. Most research has evaluated the performance after several cycles of bending, but performance in different bending states has not been extensively evaluated [107]. In one of the studies, the performance of FPSC has been studied at different radii of bending curvature. For a radius lower than 1 mm, the performance of the FPSC was reduced by 7% to the initial PCE [114]. In another similar study, performance was reduced by

17% when the bending radius was 4 mm [97]. However, for the same bending radius, a record efficiency of 21.73% was achieved with a reduction in PCE of only 6% [115]. The performance of FPSC was further evaluated at different angles and in different bending directions. The PCE remains at 95.16% in a bending state; however, the charge density reduces when bending downward by almost 10% [116]. The FPSC performance has further improved in the bending state by introducing silica nanospheres. This improves the FPSC performance in the bending state by 7.3% and 1.7% in the upward bending state [117].

3.1.6. Organic Solar Cells (OSCs)

Organic solar cells (OSCs) have received much attention for photovoltaic applications because of their intrinsic flexibility, high throughput large-area printing, light weight, and low cost. The applications of OSCs as flexible, portable devices for indoor building-integrated PV and automotive-integrated PV make them prominent compared to all other solar-cell technologies [118]. O'Regan and Grätzel originally accomplished a novel preparation of semiconducting layers and sensitizers called dye-sensitized solar cells (DSSCs) in 1991, and a new era of PV was introduced. For OSC flexible devices, there are two key contenders for glass replacement, i.e., conductive plastics or metallic foils, both with advantages and disadvantages. Flexible conductive plastic substrates for the manufacture of flexible DSSCs comprise indium tin oxide (ITO)/polyethylene nephtalate (PEN)-ITO/PEN and FTO/PET-FTO/PET), whereas flexible metal substrates include titanium foil or wires, Ti, or stainless-steel wire, etc. [119]. Because of their strong electron affinity and mobility, fullerene acceptors have dominated OSCs for a long time. However, the fullerene acceptors' weak absorption in the near-infrared (NIR) region, low energy-level tunability, and morphological instability have hampered their development [120,121]. For next-generation organic solar cells, a high-performance fused-ring non-fullerene acceptor (NFA) called ITIC (3,9-bis(2-methylene-(3-(1,1-dicyanomethylene)-indanone))-5,5,11,11-tetrakis(4-hexylphenyl)-dithieno[2,3-d:2′,3′-d′]-s-indaceno[1,2-b:5,6-b′]dithiophene) has been developed. It has strong and wide absorption in the visible and near-infrared areas, an acceptable energy level matched with low-bandgap donor polymers, and good donor/acceptor miscibility [122]. Since then, a lot of new high-performance NFAs have emerged, and the champion power-conversion efficiency (PCE) of NFA-based OSCs has surpassed 19% in the small-area device size (<1 cm^2) [104,123–125]. The most common approach for the solution-based fabrication of efficient OSCs is the spin-coating method because of its simplicity and high reproducibility of film thickness and morphology in small-area preparation, along with other techniques like blade-coating, slot–die coating, Gravure printing, and inkjet printing. However, not all these approaches are suitable for large-area production because film uniformity, thickness, and crystallization cannot be controlled during deposition [126–128]. Another key factor for the efficient photovoltaic and mechanical performance of OSCs is the selection of flexible transparent electrode (FTE) because it should have strong mechanical bending durability, high optical transparency, low surface roughness, and low sheet resistance [129].

With respect to recent progress in OSCs, PM6:BTP-BO-4Cl (PM6: Poly[(thiophene-2,5-diyl)-alt-(2,5-bis(2-hexyldecyl)-4,6-dioxo-1,3,5-triazine)] + BTP-BO-4C: Benzotriazole-based acceptor) absorbing material was used by Chen et al. using the layer-by-layer inkjet printing (LBL-IJP) technique for the fabrication of small-area OSCs with a PCE of 13.09% by balancing nanoscale phase aggregation and gradient vertical phase separation morphology. Zhang et al. [127] fabricated small-area OSCs with the inverted structure, which was constructed on PM6:CH7 (PM6: Poly[(thiophene-2,5-diyl)-alt-(2,5-bis(2-hexyldecyl)-4,6-dioxo-1,3,5-triazine)] + CH7: Small-molecule non-fullerene acceptor) using the blade-coating approach, and it demonstrated a PCE of 17.49%, which is typically associated with

the high and balanced mobilities of charge carriers and suitable shape. A large-area module with the same active layer of 25.2 cm^2 was formed using the non-halogen solvent OX, which showed a PCE of 14.42%. A bilayer-merged annealing (BMA)-assisted blade-coating method was applied by Fan et al. [130,131] to synthesize a high-performance OSC module based on PM6:BTP-BO-4Cl with a PCE of 14.79% with an active area of 18.73 cm^2. BMA technique successfully handled enhancing film coverage as well as electronic and electric contacts of multistacked photoactive layers. Zhao et al. used a slot–die-coating approach using halogenated chlorobenzene (CB) and hydrocarbon solvents for an efficient PM6:Y6 (PM6: Poly[(thiophene-2,5-diyl)-alt-(2,5-bis(2-hexyldecyl)-4,6-dioxo-1,3,5-triazine)] + Y6: A-Class NFA (non-fullerene acceptor)) blend-absorbing layer for small-area cells achieving PCEs of 15.2%, 15.4%, and 15.6% for chlorobenzene (CB), 1,3,5-trimethylbenzene (TMB), and o-XY solvents, respectively, by optimizing the aggregation state and film formation [132]. A D18:Y6:BTR-Cl (D18: A wide-bandgap polymer donor + Y6: A-Class NFA + BTR-Cl: Chlorinated small molecule) active layer was produced by Zhao et al. by improving the molecular crystallinity and vertical phase separation of the ternary blends to achieve a PCE of 17.2% for small-area cells [133]. An ultra-thick layer of 1000 nm of absorbing material PM6:BTP-4Cl was synthesized by Ma et al. [134] with a blade-coating approach, providing a PCE of 12.1% by lowering the trap-assist recombination, increasing carrier lifetime, and thus providing a much higher short-circuit current density in the device. For an active area of 4 cm^2, a promising efficiency of 10.1% was achieved for the same specifications. In addition, a PCE of 15% was achieved for 328 nm thickness of the same absorbing layer device. A PM6:BTP-eC9 (PM6: Poly[(thiophene-2,5-diyl)-alt-(2,5-bis(2-hexyldecyl)-4,6-dioxo-1,3,5-triazine)] + BTP-eC9: Benzotriazole-based acceptor) active layer was used for the fabrication of cells and enhanced performance by synergistic effects of broader light absorption, reduced voltage loss, improved charge transport, and suppressed recombination by the addition of a novel acceptor L8-BO-F (fluorinated benzotriazole-based NFA) into the host system. A PCE of 18.2% was achieved by this device [135].

For flexible organic solar cells FOSCs, we can dive into current trends starting by looking at Yue et al. [136], who synthesized FOSCs with ITO/ZnO/P2:PCBM (P2: Polymer donor + PCBM: [6,6]-phenyl-C61-butyric acid methyl ester)/PEDOT:PSS (Poly(3,4-ethylene dioxythiophene):Poly(styrene sulfonate))/Ag structure by spin-coating approach and achieved 2.84% PCE. The flexible organic solar cells with architecture FlexAgNE/ZnONPs/PFN-Br/D1:A1:A4 (D1: Donor polymer + A1, A4: Acceptor molecules)/MoO_3/Ag were fabricated with various types of donors and acceptors by Sun et al. using the spin-coating method, achieving a PCE of 13.1% for single-junction flexible organic solar cells. Qin et al. [137] manufactured flexible OPVs with Ag grid/AgNWs:PEI-Zn/PBDB-T-2F:Y6:PC71BM (PBDB-T-2F: Donor polymer + Y6: Acceptor + PC71BM: [6,6]-phenyl-C71-butyric acid methyl ester)/MoO_3/Ag structure with a PCE of 13.2% (54 cm^2) based on PET/Ag grid/AgNWs:PEI-Zn (silver nanowires (AgNWs) coated with polyethylenimine-zinc) composite electrodes because solution-processed AgNW flexible transparent electrode:PEI-Zn has a smooth surface and good optoelectronic and mechanical characteristics. PEI-Zn is both conductive and transparent. Yan et al. [138] produced flexible OPVs with the following structure: PEDOT:PSS/PEDOT:PSS (4083)/PM6:Y6:PC71BM/PDINO (perylene diimide-functionalized organics)/Al, a wide-bandgap polymer donor (PM6), a narrow bandgap non-fullerene acceptor (Y6), and PC71BM as the third component to control the light absorption and morphologies of the blend films, was used which improved absorption in the range of 300–500 nm and increased photogenerated charge dissociation and extraction resulting in achieving 14.06% PCE. Song et al. created flexible OSCs with the architecture of D-PEDOT:PSS/PEDOT:PSS (4083)/D18-Cl:Y6:PC71BM (D18-Cl: Chlorinated donor

polymer + Y6: Acceptor + PC71BM: Fullerene acceptor)/PFNDI-Br-Ag (polyfluorene naphthalenediimide bromide with silver) by adding a third material, a PC71BM molecule, to reduce crystallization without affecting the electron mobility of the absorbing layer and decreasing the rigidity of the active layer and making it mechanically flexible. They achieved PCE of 15.5% for this type of flexible OPV [139]. Flexible OPV with ITO/PEDOT:PSS/D18-Cl:G19 (a specific polymer donor whose exact formulation varies by context):Y6/PFNDI-Br/Ag were manufactured by Chen et al. using a G19 small donor in the active layer, which improved the performance of the device to obtain PCE of 15.9% [140]. Wan et al. produced flexible OPVs with the structure of PEDOT:PSS/PEDOT:PSS (4083)/PM6:Y6/PDINN/Al using the spin-coating approach while using trifluoromethanesulfonic acid CF_3SO_3H-doped transparent conducting PEDOT:PSS anode providing superior wettability, and good electrical stability. This solution-processed flexible OSC produced a power-conversion efficiency of 16.61% [141]. In flexible OSCs, to accurately regulate the reduction process of silver (Ag) in AgNW-based FTEs, an ionic liquid (IL)-type reducing agent comprising Cl and a dihydroxyl group was used by Zeng et al. [142], who used spin coating to deposit the active layer and charge-transport layers. The development of atomic-level contact between the AgNWs and the reduced Ag-induced atomic-level interaction reduced sheet resistance and improved FTE mechanical stability, resulting in a PCE of 17.52%. The structure of the FTE is PET/Em-Ag/AgNWs-IL. Ye et al. recently developed D18:N3:DOY-C4 (D18: Wide-bandgap donor polymer + N3: Acceptor + DOY-C4: Small molecule)-based flexible OSCs by introducing ductile oligomeric acceptor (DOA), which exhibited 17.91% PCE with high mechanical stability [143]. The brief summary of advantages and disadvantages of all the active materials in the above section is tabulated in Table 1.

3.2. Substrate Material Desired Properties

The key aspect of the flexibility of solar cells is exhibited through the flexible substrate. The most common commercial substrate is glass, which demonstrates high transparency and robustness. However, due to the rigidity of traditional glass, it is not suitable for FPV. Generally, to make a substrate suitable for FPV, it must have the following properties. The substrate should be mechanically robust enough that it can withstand the fabrication process and daily operating conditions. Also, it should have the flexibility to bend at different radii of curvature without any deformation. The substrate should be chemically inert to the other materials used in PV modules during the fabrication process. Moreover, it should sustain higher processing temperatures during the fabrication process of the cells. The substrate must suit the coefficient of thermal expansion of other functional layers in the solar cells. The optical properties of the substrate must be taken into consideration because it determines the cell's structural configuration. Usually, high optical transmittance or high reflectance properties are desirable for solar-cell fabrication. The above-mentioned properties are further explained below.

3.2.1. Flexibility

Flexibility is the property of a material to bend without fracture or rupture. It can be further elaborated in a way that material can be bent or rolled without plastic deformation or stretched elastically. The bendability and stretchability depend on the elastic behavior of the material. When the material undergoes elastic strain, it can retract back to its original shape when the stress is released. However, if the load applied crosses yield strength, the material moves into the plastic region, after which it is no longer recoverable. The permanent shape of the material is associated with plastic deformation. Therefore, the deformation behavior in both the elastic and plastic regions is very important for substrate design. The elastic deformation behavior of a material is usually described by

Young's modulus and elastic elongation. However, plastic deformation is described by yield strength and total elongation.

Young's modulus is the stiffness property of a material. It is usually higher for metals and ceramics and lower for polymers. The Young modulus for stainless steel is 190 GPa [144,145], whereas, for soda lime glass, the value is around 70 GPa [146]. However, for polymers such as PET, the value is 3 GPa [147], much lower than other counterparts. This makes polymer a suitable candidate for flexible substrates due to its higher stretchability and bendability. Moreover, elastic deformation for PET is approximately 10^{-2}, which is higher than that of metal foil and soda lime glass, which stays around 10^{-3}. This property makes polymer substrates more flexible. Similarly, other strength properties like yield strength and total elongation are higher for stainless steel than polymer substrates. The yield strength and total elongation for stainless steel are 250 MPa and 0.33 [148], whereas, for PET polymer, the values are 40 MPa and 0.70 [147], showing better flexibility for the latter. Thickness of the substrate is also important to achieve flexibility of the substrate. To achieve flexibility, ceramic materials such as glass and zirconia are made thinner to reduce their brittle nature. Usually, the brittle substrates are made thinner with thicknesses below 100 micrometers [149].

3.2.2. Thermal Stability

Thermal stability is another important aspect of device stability during the manufacturing of PV modules. Some materials require higher temperatures to develop bonding in the multilayer system. Stainless steel can withstand temperatures of up to 900 °C [150], whereas glass can bear a temperature of up to 650 °C [151]. However, a polymer can only withstand low temperatures due to the limitation of the glass-transition temperature. The glass-transition temperature for PET is 70 °C, whereas for PC, it is 145 °C [66]. Another important characteristic for the substrate to be easily integrated with other layers of the PV module is the coefficient of thermal expansion. The coefficient of thermal expansion (CTE) must be either lower or should have matching values of CTE with other layers of the PV modules. During the fabrication process, the substrate either expands or contracts. The mismatch between the thermal characteristic of the substrate and other layers will induce stresses followed by strains [152].

3.2.3. Barrier Properties

Solar cells and other electrical conducting materials of the PV modules are sensitive to oxygen and moisture. The substrate should act as a barrier layer to prevent the transmission of oxygen and moisture. This property varies depending upon the type of technology [153]. Organic solar cells require higher barrier properties as compared to inorganic solar cells [154]. Due to the dense packing of atoms of metals and ceramics, these substrates have lower values of oxygen transmission rate (OTR) and water vapor transmission rate (WVTR). However, for polymer substrates, the values are higher due to loosely packed polymer chains. Some polymers are hydrophobic, while some absorb water easily [155]. PET is hydrophobic, but the WVTR is high, which is 9 $g^{-2}day^{-1}$. In the case of PC, the 50 $g^{-2}day^{-1}$ as it absorbs water [156]. These values are high, and without coating or other barrier layers, it cannot fulfill the requirement for a substrate. These coatings are usually ceramic nanofillers or layers such as SiO_x, AlO_x, or SiN_x. The range of OTR and WVTR for different device packaging [157] are given in Figure 5.

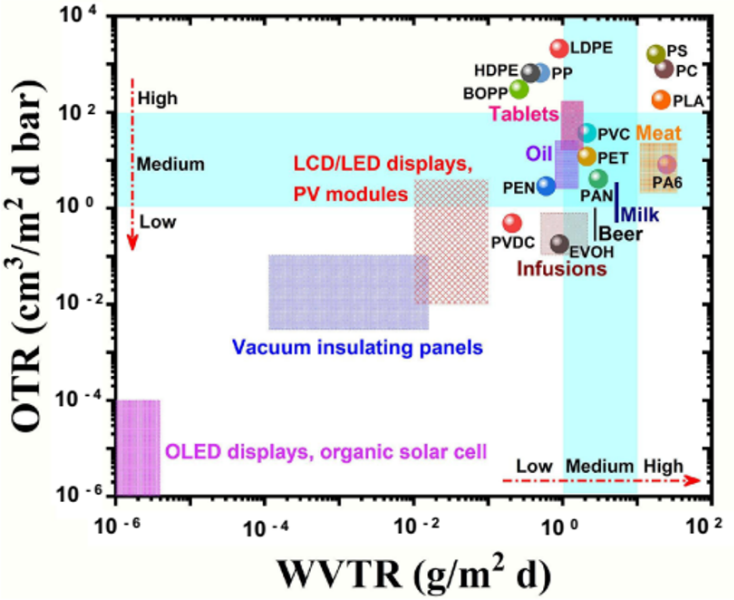

Figure 5. OTR and WVTR of different polymers used in packaging materials of different products. Source: [157].

3.2.4. Optical Properties

Optical properties are also an important consideration when choosing the substrate as it decides the cell architecture. Usually, the substrate should have higher transmittance or higher reflectance for the fabrication of solar cells [104]. To be used as the front layer, the substrate layer should have a transmittance of more than 85%. Stainless-steel substrates have reflectance in the range of 60 to 70% [158–160]. Glass substrates are transparent and have higher transparency in the range of 90% [161]. Polymer substrates like PC and PET exhibit higher transmission in the range above 85%; however, polyamide has a lower transmission rate, especially for blue light. However, it can be made transparent by changing the molecular design [162].

3.3. Substrate Materials

3.3.1. Metal Substrate

Metal substrates have higher ductility, malleability, and conduction properties, which makes them an excellent choice for substrate materials. Due to these unexceptional properties, metal substrate less than 125 µm is used as a flexible substrate for flexible solar cells. It can withstand higher temperatures during the fabrication process. It has low CTE, which makes it resistant to chemical and thermal degradation. It acts as a barrier layer to prevent oxygen and humidity permeation [163–167].

Several metal substrates have been used as flexible substrates, such as stainless steel, titanium, molybdenum, copper, and aluminum [168]. Each one has its limitations. Stainless-steel-based metal substrates are some of the most used flexible substrates owing to their outstanding material strength properties, cost, and ease of integration properties [169]. Flexible CIGS has been widely employed on flexible stainless-steel substrates. To decrease the efficiency loss, CIGS-based solar cells have been fabricated using the laser shaping method to cut and shape the cell on the stainless substrate [170]. Cd-free CIGS was developed on a stainless-steel substrate with multilayer zinc-based buffer layers to improve power-conversion efficiency. A power-conversion efficiency of 19.7% was achieved with reduced carrier recombination and improved charge density [171]. In another study, SiO_2 film was deposited through the co-evaporation method on a stainless-steel substrate to improve the barrier properties against different impurity elements in the substrate to

deteriorate CIGS cell performance [172]. For perovskite solar cells, stainless steel has been used, but the PCE of the devices is lower, though the stability of the device is better against heat, wear, and humidity [173]. This lower PCE for PSC on SS substrate is due to poor transparency of the metal top contacts [174,175]. Recently, polymer-coated stainless-steel substrate was used, achieving a power-conversion efficiency of 16.5% [164]. Other metals, like titanium foil, have also been used to fabricate PSC. FPSCs on a titanium metal substrate showed PCE of 7.5% [176]. $MAPbI_3$ flexible solar cells have been fabricated on titanium metal foil, achieving PCE of 15.03% by employing PDMS transparent electrodes [165].

3.3.2. Polymer Substrates

Polymer substrates have gained significant attraction in flexible PV due to their excellent flexibility and optical properties. The higher flexibility is due to lower Young's modulus and higher elastic elongation. Another important aspect of polymer is that it is cheaper and easier to process [17]. However, they are thermally less stable due to lower glass-transition temperatures and have higher OTRs and WVTRs than glass. However, thermal stability problems can be solved using low-temperature techniques like solution processing [177]. Similarly, OTR and WVTR problems can be solved by employing barrier coatings on the polymer substrate. Common barrier coatings include silicon oxide (SiO_x), titania (TiO_x), aluminum oxide (AlO_x), and silicon nitride (SiN_x) [178]. Polyethylene tetraphtelate (PET) and polyethylene nephtalate (PEN) are widely used commercially available thermoplastic resins used as substrates in flexible PV modules. They exhibit excellent optical properties, are low-cost, lightweight, and usually stable below 200 °C. They have optical transmittance of more than 85% and 70% elongation at breakage. They are hydrophobic and have WVTR less than 9 $g^{-2}day^{-1}$ [179]. Despite lower OTR and WVTR, PET and PEN need to be coated to make them suitable for flexible PV applications. Glass-transition temperatures (T_g) for PET and PEN substrates are 78 and 120 °C, respectively [147]. The higher thermal stability of PEN as compared to PET is due to the presence of a naphthalene ring in place of a benzene ring in the latter. Both materials undergo significant deformation above 200 °C [177]. Both PET and PEN degrade when exposed to UV [180,181]. PET is also stable and durable compared to PEN. Furthermore, PET is six times cheaper than PEN. Recently, a perovskite solar cell was developed on a PET substrate with a PCE of 32.5%, and retained its 80% PCE after 1000 bending cycles [182]. Polycarbonate has gained attraction for PV substrates due to its higher toughness, heat resistance, and higher optical transparency [183]. The glass-transition temperature of PC is around 150 °C. It has a higher flexure modulus of 2.4 GPa. However, it has lower surface energy and hence gives poor adhesion and low wettability [184]. Polyimide PI has high thermal stability, and its glass-transition temperature remains above 350 °C; however, its optical transparency fades as it absorbs light at a lower wavelength in the visible range [185].

3.3.3. Ceramic Substrates

Glass as a substrate material benefits from lower chemical contamination, lower weight, and lower roughness than metal substrates, and higher temperature resistance and efficient protection against water and contamination compared to polyamide films. Moreover, glass could lead to the fabrication of solar cells for new applications, for example, where a combination of mechanical flexibility and partial optical transparency is needed [186]. Ultrathin borosilicate glass (UTG) substrate has been widely used as a substrate for flexible solar cells [187]. Compared to a conventional glass substrate, its thickness is below 100 μm. UTG is resistant to chemicals and heat and has low surface roughness and better barrier properties than polymer substrates. However, due to lower ductility, it has a limited bending radius [188]. Willow glass by the Corning company

is the most commercially used glass substrate. It can withstand temperatures of up to 600 °C with a WVTR value below 3×10^{-7} $gm^{-2}day^{-1}$ and can bend up to a radius of 100 mm [151,189]. Flexible glass substrates are cheaper and can be easily mass-produced using the roll-to-roll process [190]. A flexible glass substrate has been used for different kinds of thin-film technologies. Flexible CdTe/CdS thin-film solar cells were developed by achieving a PCE of 10.9% [191]. Recently, a water-assisted lift-off approach has been used to fabricate flexible CdTe-based solar cells, achieving a PCE of around 12.6% [192]. Similarly, CdTe has been fabricated on UTG, attaining a PCE of 14.7% with a bending radius of 32 mm using metalorganic chemical vapor deposition [193]. Flexible perovskite solar cells have been developed on a willow glass substrate using the roll-to-roll process. These perovskite halide solar cells achieved a PCE of 18.1% [194,195]. Using the Doctor blade-coating technique, flexible perovskite film was developed on willow glass, achieving a PCE of 19.5% [151]. Moreover, glass zirconia has also been used as a substrate for flexible solar cells. However, it is heavy, expensive, and has poor surface roughness, which makes it a less favorable substrate [196]. The summary of the strengths and weakness of substrate materials used for PV is given in Table 2.

Table 2. Strength and weakness of substrate materials used for flexible PV.

Substrate Material	Strength	Weakness
PI	Good thermal stability up to 350 °C Lightweight with good flexibility and mechanical durability (tensile strength 200 MPa) Transmittance 80% in visible range	Low transmittance 80% in visible range Higher material cost Degradable under UV
PET	Lightweight Optical transparency of 90% in the visible range Low cost High ductility	Prone to UV Moderate barrier to oxygen and moisture Low thermal stability 120 °C
PEN	Higher thermal stability 200 °C Higher ductility Lightweight Transparency 85–90%	Moderate moisture and oxygen barrier Prone to UV Higher cost
Glass	Higher thermal stability 300 °C UV and Corrosive resistant Cheap Excellent barrier properties against oxygen and moisture	Brittle Lower ductility and Mechanical strength
Metals	Higher thermal stability 600 °C Excellent barrier against oxygen and moisture Higher ductility	High surface roughness Prone to corrosion Higher cost
Paper	Low cost Lightweight Recyclable	Low thermal stability Lower mechanical strength Low transparency

3.4. Flexible Transparent Electrodes

Transparent electrodes are a vital component that contributes significantly to the performance of the device in most solar cells. The development of transparent electrodes for flexible solar cells also requires that these must be flexible, lightweight, low-temperature solution process, stable, and low cost without compromising on the electrical properties of these electrodes. The creation of a superior bendable electrode, particularly for the top transparent electrode instead of the opaque bottom electrode, is a critical hurdle in attaining flexible photovoltaics [197]. Currently, research is being carried out on several types of transparent flexible electrodes, which are briefly described below.

3.4.1. Transparent Conductive Oxides

These are wide-bandgap transparent conductive oxide materials. The most widely applied transparent conductive oxides for solar cells are indium tin oxide (ITO), indium zinc oxide (IZO), fluorine-doped tin oxide (FTO), aluminum-doped zinc oxide (AZO), and W-doped indium oxide (IWO) [194,198,199]. The temperature for processing the FTO is very high, so it is not suitable for flexible solar-cell substrates; however, the synthesis of the IZO layer can be done at lower temperatures like 100 °C. However, ITO, AZO, and IWO electrodes can be deposited at room temperature. It has been observed by researchers that a chemical reaction occurs of AZO with the perovskite absorbing layer, hence decreasing its efficiency [194]. IZO demonstrates lower sheet resistance, whereas ITO produces high current density because of higher transmission. However, these both have a brittleness that makes them difficult to bend and can break while being bent. Recently, IWO electrodes have been fabricated, which have shown better efficiency as compared to those made with ITO because of their higher transmission and bigger work function [200,201]. ITO is mostly used for flexible solar cells because of its low-temperature process of synthesis, stability, high transmission, and its band structure is very well matched. FPSCs with PCE values greater than 20% are typically created on polymer/ITO substrates that are commercially available [202,203]. It is costly (50–60% of the whole cost) because of vacuum-based or sputtering deposition techniques. High surface roughness can cause current leakage, and chemical suitability with substrate also affects the performance of the device. This means there is a lot of room for development in the optical, electrical, and mechanical aspects of the ITO. Decreased thickness of ITO is helpful for its mechanical flexibility. Sputtering causes amorphous thin-film production, whereas an in-line-type vertical plasma arc ion-plating method was helpful to obtain a smooth surface with low sheet resistance of the film and high optical transmission [200]. Optimization of the structural architecture of the ITO electrode is also advantageous for improving light utilization. ITO is the most popular electrode for flexible solar cells as a bottom electrode because the ITO top electrode is typically difficult to produce due to destructive manufacturing processes or sophisticated techniques that are unsuitable for industrial production [204].

3.4.2. Metal Wanowires and Metal Films

Metallic nanostructures, such as metal nanowires, metal meshes, and ultrathin metal films (UTMFs), have great electrical conductivity and wide optical transparency, making them ideal candidates to replace ITO electrodes in FPSCs. As they have a very low cost of manufacturing and excellent optoelectrical capabilities, silver nanowires (AgNWs) are seen as the most favorable metal nanowires. The very flexible AgNWs, which are used as transparent electrodes, can help to develop roll-to-roll manufacturing techniques, and, because of their very low sheet resistance, around 80–90%, the transmittance is almost equivalent to ITO. Reduced chemical stability, higher surface roughness, inadequate coverage (lower than 40%), high connection resistance, and small adherence of AgNWs on substrates made by polymers are some of the significant concerns with AgNWs [142,205]. Also, the reaction between halide perovskite and silver can degrade the electrode. Corrosion and oxidation will occur if the silver nanowire electrode is exposed to air. Surface roughness also affects the performance of the solar cell. Depositing barrier layers or using special fabrication techniques can help to achieve a smooth surface, but this barrier layer should have good ion impermeability, better robustness in mechanical terms, and high transparency for radiation so that the extra energy losses can be minimized [206]. As above, the AgNWs layer, fluorine-doped ZnO (FZO), displayed increased conductivity and chemical and mechanical stability [207]. The usage of ITO and ZnO layers has also shown promising results in these cases. PEDOT:PSS can also be used as an interlayer between AgNWs and

the absorbing layer due to its high mechanical flexibility. Covering the exposed region and connecting the junctions of the silver nanowire can increase the flatness of the surface, substrate adhesion of the nanowires, and electrical conductivity. A large-scale process of roll-to-roll slot–die was used to create transparent electrodes of AgNWs/PEDOT:PSS on PET substrates. In FPSCs, which are TCO-free, with great mechanical flexibility, a PCE of 11% was attained [184]. The fabrication of a composite electrode named PH1000/AgNWs on the substrates of transparent biomass polylactic acid was reported, which had greater than 82% average transmittance in the region of 400–800 nm and demonstrated a very low sheet resistance with a value of 25 ohm/sq. Additionally, the FPSCs that are based on this composite electrode displayed a reasonable PCE of 11.44% while remaining flexible [208]. Apart from PEDOT:PSS, AZO and graphene can also be used for this purpose. Coating additional materials, on the other hand, would change the work function of AgNW electrodes. Whenever the top electrode application is carried out by AgNWs, semi-transparent PSCs can be produced. The solvent, which is used as a solution for solution-processed AgNWs, on the other hand, may harm the layers that are fabricated under it in PSCs. Rather than spin coating and blade coating, the spray coating approach with a solvent like isopropyl alcohol (IPA) with a low boiling point and an ultrafast drying procedure is a viable option for producing AgNWs top electrodes [209].

The usage of metal meshes makes them an intriguing contender to have a competition with the widely used TCO electrode, particularly in solar devices with flexibility, because of their excellent electrical conductance aspect, strong transmittance of light, and flexibility in mechanical properties. Various metal meshes, like silver, gold, copper, and nickel mesh, are commonly applied with other transparent conductive materials so that extremely well-performing composite electrodes can be fabricated [210]. Because of their superior optical and electrical performance, Ag mesh/PEDOT:PSS are being established so that these can be helpful to change transparent electrodes like ITO/PEN used in flexible PSCs [211]. The device's stability is hampered by the existence of corrosion between the silver electrode and the absorbing perovskite materials, but the adjustment of the PH1000 material with the ammonia and polyethyleneimine could assist in terms of a barrier over the silver grid electrode so that it can eliminate the redox reaction efficiently because the adjustment of the pH can be performed by the ammonia and polyethyleneimine can reduce the value of PH1000 before Ag. Consequently, their usage increased the PCE of comparable devices to 14.52% from 3.3% [208].

Photolithography is being used for the development of Ag mesh, but it is costly and time-consuming. Cu grids were photolithographed onto PET substrates to generate a hybrid electrode using the layer of PH1000. The FPSCs produced with a top electrode made of copper were 13.58% efficient, preserving more than 90% efficiency of the basic device [126]. Yang and colleagues created silver grids with excellent clarity via a dense particle-stacking approach. The grids with PET/PDMS/Ag stack had 7.9 Ohm/sq. sheet resistance and a transmittance of greater than 85% (in the range from 395 nm to 900 nm), whereas the matching FPSCs showed an excellent PCE of 18.49% [99]. In the use of flexible electronics, the effective material that can be used to stop ion diffusion as a barrier layer is graphene. The Ni-based mesh electrode is comparatively more stable as on its surface, it can produce nickel oxide. Wang et al. fabricated a transparent bottom electrode, and it was made using a PET/Ni-mesh/PH1000 configuration that has a transmittance of approximately 85–87%, also providing a low sheet resistance of 0.2–0.5 Ohm/sq., which is, in terms of performance, quite better than the silver mesh counterpart, which exhibited 17% efficiency and strong mechanical durability [141]. When transparent electrodes, which are metal mesh, are used as top electrodes, heat conductivity that is not uniform cannot be considered to be an issue. However, there are certain issues with manufacturing metal

mesh as the production methods can typically harm the functional layers that are below these electrodes [126].

Outstanding electrical and mechanical characteristics, great bending stability, and even foldability make ultrathin metal films a good choice for flexible electrodes. The two most important requirements for UTMF electrodes (such as Cu, Ag, and Au) are good optical transmission and high electrical conductivity to successfully have charge collection, but these are dependent on the film thickness [212]. Through magnetron sputtering or thermal evaporation, UTMF electrodes may be utilized on polymer substrates as a transparent bottom electrode. Fabrication technologies that use solutions are considered more suited to UTMF mass manufacturing. Feng et al. used a vapor deposition approach to fabricate perovskite films on the substrates which were UTMFs-based. The matching (7 nm) silver film anode showed a smaller amount of sheet resistance and light transmittance of the normal range. As a result, a 9.05% efficiency of the device with high flexibility in terms of mechanical properties was achieved for the devices with flexibility, with 74% of the initial PCE remaining after applying bending 2000 times at a very small value of radius, 3.5 mm [213].

Metal films become opaque and extremely conductive as their thickness grows to 60–100 nm, and these are used in FPSCs mostly as top electrodes. Thermal evaporation is often used to manufacture metal films such as Cu, Ag, Al, and Ag. The metal film's uniform and dense shape allows for efficient interaction with the charge-carrying layer. The fundamental and environmental durability of electrodes fabricated by metal film, on the other hand, is concerning since the metallic connections are quickly disrupted by the perovskite layer's iodide [8]. Au has a higher chemical inertness than aluminum and silver. Still, the stability of systems for longer times depending on Au electrodes remains unsatisfactory. It is observed that under 70 °C, in the perovskite layer, the silver film can diffuse, and it will result in permanent performance loss [214]. Insertion of a barrier layer consisting of thin chromium between HTL and Au may increase PSC stability for a longer time. However, the buffer layer's barrier performance may not last for many years of operation. Under heat annealing or light irradiation, the top electrode of copper can remain stable even if it has a direct interaction with perovskite [215].

3.4.3. Polymer-Based Electrodes

The polymer that conducts electricity, known as PEDOT:PSS is also a viable substitute for the ITO. As an electrode, PEDOT:PSS offers various benefits, including its processing with solution, excellent transmittance of light, great flexibility, and even stretchability [216,217]. It is ideal for the process of roll-to-roll, and the customizable work function allows for the use of both cathode and anode materials. Using dimethyl sulfoxide (DMSO) and Zonyl FS-300 doped DMSO, Kaltenbrunner et al. presented an interesting study. In FPSCs, a PEDOT:PSS electrode is used. They were able to fabricate (3 μm) ultrathin, extremely flexible, and airtight FPSCs on PET substrates of 1.4 m thickness with 12% efficiency [216]. Hu et al. synthesized modified PEDOT:PSS using glycol and Zonyl FS-300 performing as a transparent electrode with high conductance and a polystyrene-doped nano cellular PEDOT:PSS used as an HTL in FPSCs to synchronize and improve mechanical elasticity and light utilization. Devices with 12.32% efficiency were made for FPSCs to be produced on a large scale with exceptional flexural endurance, providing greater than 90% of the PCE of the reference device remaining after being applied to 1000 cycles with a very low value of the radius of 2 mm [217]. Zhang et al. were able to produce PDMS transfer-printed PEDOT:PSS electrodes in their FPSCs. The devices that were fabricated on PET substrates gave not only 10.3% efficiency but also good flexibility in terms of mechanical aspects as the high conductivity was able to achieve HNo_3-modified PEDOT:PSS [218]. Due to the complexity of the process, the transfer-printing approach is not considered ideal

for roll-to-roll manufacturing. At the same time, powerful acids are notorious for causing environmental and safety difficulties. The acid-free method for increasing PEDOT:PSS conductivity by combining post-treatment and polar solvent doping is a preferable option. The fabricated PEDOT:PSS layer, as explained above, has sheet resistance in less value and a 76% average optical transmittance, making it most suitable for the applications of transparent electrodes as flexibles [219].

Song et al. used a roll-to-roll approach to create PEDOT:PSS with high-conductivity network electrodes on PET substrates. Because of the network topology, the PEDOT:PSS film demonstrated outstanding flexibility and optical transmittance. The FPSCs that use it as a transparent electrode had stabilized efficiency values of 19.0% and 10.9%, respectively, with 0.1 and 25 cm^2 of effective areas. The equivalent devices also demonstrated exceptional stability of cells and mechanical flexibility, with 85% of the starting efficiency retained after applying 5000 bending cycles at a curve of 3 mm [220]. Later, by passivating perovskite grain boundaries, they increased the efficiency of FPSCs created with PEDOT:PSS to more than 20% using 1.01 cm^2 effective area [221]. Apart from the common usage of PEDOT:PSS as a bottom electrode, there have been few studies using it as a top electrode because the aqueous solutions are used for the deposition of PEDOT:PSS, which is very harmful to the underlying absorber layer. PEDOT:PSS is normally used on PDMS substrates for the application of bottom electrodes in FPSCs, and the top electrode, the electrode of PEDOT:PSS, is made using a lamination process of film transfer. As a result, the FPSCs were able to show 15.1% efficiency of cells with small-area devices and 7.91% of cells with large-area devices of 56 cm^2. Furthermore, no efficiency drop was seen after applying 5000 bending cycles at 2 mm, a very small radius, and only a 10% decrease was observed after applying it [220]. The polymer that conducts electricity, PEDOT:PSS, provides a unique flexible electrode option in FPSCs, with efficiencies of more than 20%, equivalent to the ITO counterpart. PEDOT:PSS seems more suited to its applications in flexible solar devices than brittle ITO electrodes due to its solution processability and superior mechanical flexibility. The fundamental issue with the use of FPSCs is their low-value electrical conductivity, and that can be enhanced by doping them with polar solvents, ionic liquids, and acids [222].

3.4.4. Carbon Based Electrodes

Carbon content is abundant on Earth and has superior chemical robustness. It also shows flexibility and can be directly used in a roll-to-roll approach. Carbon nanomaterials, which are usually known as carbon nanotubes (CNTs) and graphene, are potential alternatives for the ITO electrodes in flexible solar cells [213]. Transparent carbon nanomaterials with outstanding optical and electrical properties outperform their ITO counterparts. Because they show very high resistance to temperature, superior performance in terms of optical and electrical usage, stability in the atmosphere is exceptional, and scalable production capabilities, CNTs have significant potential because these are very inexpensive and an efficient substitute for ITO, which has a high cost and also it is very fragile. Furthermore, CNTs have high repeatability due to their simple synthesis and simple transfer approach. As it offers very low production cost, high values of efficiency, and scalability, floating catalyst chemical vapor deposition is a popular approach for the synthesis of these CNTs. Except for electrodes in PSCs, CNTs can serve a variety of functions, including charge-transport layers [223,224], perovskite additives [225–227], and interlayers. CNTs can also be divided into distinct groups based on the number of concentric graphene cylinders. Single-walled carbon nanotubes (SWNTs) are considered the most basic type, consisting primarily of a single graphene cylinder [228]. FPSCs were demonstrated on the substrates of PET/diluted HNO 3-doped SWNTs yielding 5.38%-efficient solar cells [229]. While doing a comparison to HNO_3 ionic dopants, the transition metal oxide MoO_3 is excellent

and can be counted as a dopant that is stable for SWNTs for creating a substantial effect of p-type doping. The device performance of the doped SWNTs-based FPSCs was 11.0% when a thin 2 mm layer of MoO_3 was placed to the SWNTs electrode [230]. There are also double-walled carbon nanotubes (DWNTs) and multi-walled carbon nanotubes (MWNTs). In contrast to hydrophobic SWNTs, MWNTs can be processed with solution. DWNTs, which consist of two overlapping carbon cylinders, can give the combined benefits of MWNTs and SWNTs, displaying good transparency along with conductivity while keeping processability based on solution and chemical stability. The optical transmittance of MWNT film is not greater than that of SWNT over a visible area. Furthermore, PSCs that are made by modifying the DWNTs, which have very smooth film morphology and very good energy-level alignment compared to SWNTs, obtained a greater performance, reaching 17.2%, suggesting the potential of DWNTs in flexible solar devices [231].

In comparison to carbon nanotubes, graphene with a single atom is comparatively smooth, giving more current and transparency over a wider region of the wavelength range. The electrode of the 2-layered graphene based on PET, for example, has a 300 ohm/sq. sheet resistance and has an optical efficiency of 87.3% transmittance at 550 nm wavelength [232]. Graphene films have a greater transmittance than ITO, especially if we look at the near-infrared spectrum. Theoretically, graphene carries carrier mobility of a very high amount, but realistically and practically, it is constrained by the quality of the film production and is significantly lower than the theoretical value. Stacking of the graphene sheets and usage of chemical doping can be thought of as two key ways to increase graphene conductivity by lowering sheet resistance. Doping effectively affects both the current production and Fermi level of the material, and different dopants in this case that are commonly used include MoO_3, and $AuCl_3$.MoO_3 is a favorable p-type dopant that also converts the hydrophobic graphene surface to hydrophilic to ensure the construction of the subsequent films, such as PEDOT:PSS [233]. With the doping of the MoO_3, Choi and colleagues used a wet transfer transparent electrode of the 2D graphene material with PEDOT:PSS, which provided coverage as the HTL. The energy levels were made quite better aligned, and by giving higher transmittance, the FPSCs created with the MoO_3/graphene were able to achieve 16.8% efficiency and also with almost negligible hysteresis of the device, which makes it a unique substitute to the devices, which are based on ITO electrode (17.3%) [233].

Inverted FPSCs that are independent of the TCO have been demonstrated using MoO_3 doped SWNTs or MoO_3 doped graphene instead of ITO and comparing their performance and mechanical resilience. Because of their improved film shape and higher values of the optical transmittance, FPSCs fabricated with graphene materials outperformed FPSCs that were SWNT-based with 11.0% efficiency [230]. Researchers used a new transparent electrode by the usage of PET substrates and applying $AuCl_3$ doped with one-layer graphene and with 3-aminopropyl triethoxysilane (APTES) that was basically used as an interlayer. It was able to fabricate devices with 17.9% efficient cells showing excellent flexural endurance [234]. Heo et al. produced FPSCs that were very good in terms of efficiency and stability, demonstrating 18.3% efficiency, a transparent electrode on APTES linked PDMS substrates using a trifluoromethanesulfonic acid (TFSA)-doped graphene sheet [165]. The inadequate adhesion between graphene and substrates causes less contact and significant deformation in terms of mechanical strength during flexural experiences, which is a challenge in the application of graphene. More graphene contacts must be developed to realize ultra-flexible devices such as the APTES. Flexible solar cells based on carbon nanomaterial electrodes are often less efficient as compared to FPSCs which use ITO. This is mostly owing to the low current generation produced by CNTs' high inter-tube contact resistance and defective shapes of graphene. The many dopants can be used to improve the current generation of CNTs and graphene, such as PEDOT:PSS,

acids, and MoO_3, and better adhesion of CNTs with a substrate is to be explored to achieve mechanically robust device [235,236].

4. Fabrication Techniques for Absorbing Materials in Flexible Solar Cells

There is a variety of materials that can be used as an absorbing layer in flexible solar cells. Depending upon the applications of solar cells and operating conditions significantly impact the choice of this layer material. In this section, we will focus on the most common materials that are used for this purpose and their fabrication approaches. i. Amorphous silicon solar cells ii. CIGS solar cells iii. Organic solar cells iv. Perovskite solar cells

4.1. Amorphous Silicon Solar Cells

To make effective flexible solar cells, hydrogenated amorphous silicon (a-Si:H) can be a potential absorbing layer. Plasma-assisted chemical vapor deposition (PECVD) can be used to deposit the a-Si:H layer in most cases, as well as, to a lesser extent, chemical vapor deposition (CVD). The best-recorded efficiency of a single-junction a-Si:H solar cell is 10.2%, corresponding to an active area of 1 cm^2. For multi-junction devices with a triple-junction solar cell based on a-Si:H/nc (nano-crystalline)-Si:H/nc-Si:H, the best-validated efficiency is 14% for an active area of 1 cm^2, and for double junction based on a-Si:H/nc-Si:H solar cells the best PCE is 12.7% for 1 cm^2 [237]. The best confirmed efficiency for Si:H/nc-Si:H is 14% (1-cm^2), and (2) a-Si:H/nc-Si:H 12.7% (1-cm^2) [168]. With an efficiency of 12.3%, the champion large-area module (14.322-cm^2) a-Si:H/nc-Si cell was validated. The relatively tiny performance discrepancies between laboratory-scale solar cells and commercially produced modules demonstrate the technology's maturity. However, no major validated records in cell efficiency have been set in the recent two decades [14]. Zhang et al. used the sol–gel-based nanoimprinting method for a-Si deposition on polyimide (PI) substrates and obtained 8.17% PCE [88]. Plasma-enhanced chemical vapor deposition (PECVD) at very high excitation frequency (VHF), 50–150 MHz on PEN substrates produced amorphous silicon a-Si:H thin-film solar cells with a PCE of 8.8% [238]. Cao et al. also employed the PECVD method to fabricate a-Si flexible solar cells and were able to obtain 7.26% PCE [239].

4.2. CIGS Solar Cells

Cu(In,Ga)Se (CIGS) materials have fewer flaws within a solid film than a-Si:H materials and are similarly appealing for flexible solar applications. CIGS-based materials have quickly risen to the forefront of flexible solar-cell technology. A bandgap of more than 1.50 eV can be achieved by changing the gallium content [240]. However, most CIGS bandgaps are less than that. Vacuum co-deposition is used to create the best-performing CIGS flexible solar cells, allowing for easy tweaking of the chemical composition and the thickness of the CIGS layer. This allows graded bandgap designs to assist photo-carrier movement while also achieving high energy conversion. To date, the great majority of studies have demonstrated that sputtering deposition and salinization-based processes may yield highly efficient flexible CIGS solar cells [12]. Various passivation technologies have been used to eliminate flaws in CIGS solar cells to increase device performance even further. The incorporation of alkali elements (sodium, potassium, and cesium, for example) has been extensively used for defect passivation of the CIGS layer. A record efficiency of 22.6% has been established for defect passivation using potassium, and CIGS layers were co-evaporated [241]. Chang et al. used multistage co-evaporation of the CIGS absorbing layer and implemented a tunnel junction, hence achieving 15.57% PCE [242]. The efficiency of larger commercially available modules remains around 16%. In a study by Luo et al., a novel Ga growth profile was established and built to improve the performance of flexible CIGS solar cells, which co-evaporated with Cu and Se in the second phase of the well-

known "three-step co-evaporation technique". With a thickness of about 1.6 mm, the best flexible CIGS solar cell reaches an amazing efficiency of 18.93% [243]. This was achieved using PI substrates. Multistage co-evaporation was used to deposit CIGS absorber layers on a PI substrate, and postdeposition treatment with strong alkali was used to achieve a PCE of 20.8% for the area of 0.5 cm^2 [244]. EMPA established a record efficiency of 17.7% on a flexible SS substrate utilizing a three-stage co-evaporation technique for CIGS absorbing layers for module-level fabrication [245]. The highest efficiencies of different flexible solar cells fabricated by different techniques are shown in Table 3.

Table 3. Highest PCE (%) achieved by each technique for flexible solar cells.

Technique	Year	PCE (%)	Area [cm^2]	Active Layer	Reference
PECVD	2023	23.35	NA	c-Si	[211]
Spin coating	2021	25.83	0.16	$FAPbI_3$	[246]
Slot–die coating	2021	20.8	0.16	$MAPbI_3$	[237]
Spray coating	2020	20.6	1	CsMA-based	[247]
Screen printing	2020	15.89	0.1	$MAPbI_3$	[248]
Inkjet Printing	2021	21.6	0.105	$Cs_{0.1}MA_{0.15}FA_{0.75}Pb(I_{0.85}Br_{0.15})_3$	[249]
Flexographic Printing	2022	15.3	0.134	$Cs_{0.15}FA_{0.85}PbI_3$	[250]
Blade coating	2021	21.09	0.16	$MAPbI_3$	[251]
Gravure Printing	2020	19.1	0.096	$FAPbI_3$	[252]
Co-evaporation	2019	20.8	0.5	CIGS	[244]
Spin coating	2020	17.35	0.062	PBDB-T-2F:BTP-eC9:PC71BM	[245]

4.3. Organic Solar Cells

Considering the swift development of OSCs, the PCEs of monolithic large-area OSCs (active area > 1 cm^2) fall behind that of small-area devices owing to the excessive sheet resistance of transparent electrodes, significant defect densities of thin active layers, large geometric fill factor (GFF), and other factors. At the same time, to maintain efficiency, it is vital to identify appropriate approaches for massive production and understand how to link modules in series efficiently. Tsao et al. used various fabrication approaches for large-area flexible OPVs, and the most favorable technique in their case was slot–die coating, which produced cells with 7.8% PCE while other approaches had less than 5% PCE [253]. Ternary heterojunction techniques have appeared to be an effective method for increasing the efficiency of organic solar cells (OSCs), and a spin-coating strategy was employed to deposit the absorbing layer, resulting in a PCE of 14.07% for a flexible device with area of 0.4 cm^2 [138]. Also, spin-coated ultra-flexible and ultra-lightweight organic solar cells showed PCE of 15.5% for an area of 0.4 cm^2 [139]. Fine morphology tuning of the device was carried out, the spin coating was used to deposit the main absorbing layer of OSCs, and it produced 15.9% efficient cells [140]. Flexible OSCs were spin-coated and demonstrated 16.61% PCE based on a transparent conducting PEDOT:PSS anode doped with trifluoromethanesulfonic acid (CF_3SO_3H) [141]. Open-air meniscus-coated OSCs achieved a high PCE of 16.77% [172]. Slot–die printing is additionally a viable meniscus printing methodology that produces high-efficiency large-area OSCs, and it is considered to be a particularly prospective manner for roll-to-roll (R2R) manufacture of organic photoelectric devices. The PCEs of the OSCs manufactured with Gravure printing-based electrodes were 15.28% and 13.61% based on 0.01 and 1 cm^2, respectively [254]. Organic solar cells need fine control over ink patterns, which inkjet printing technology presents. Meanwhile, all inkjet printing and all air processing processes can be used to realize OSCs with a good PCE of 5%. Spray coating is a surface coating process that involves dispersing ink into even and small droplets with a spray pistol or disk-type atomizer. Screen printing normally employs a screen as a base foundation for producing patterned screen plates using the photosensitive plate-making methodology. Screen printing has

demonstrated potential in the large-area fabrication of OSCs due to its large area and low-cost production for organic solar modules; it can also be compatible with the standard R2R printing technology. Brush printing has demonstrated impressive in the preparation of high-performance OSCs, owing to the beneficial effects of elevated material usage rate, quickly obtaining ready speed, precise control of film thickness, well compatibility with R2R technology, and flexible substrates, despite insufficient research. c-Si-based flexible solar cells on module level recently showed 23.35% and those were fabricated by PECVD technique [211]. Highest efficiencies of different flexible solar cells fabricated by different techniques are shown in Table 3.

4.4. Perovskite Solar Cells

The most important point towards achieving outstanding performance in perovskite films is the development of high-quality perovskite films with great mechanical durability, robust flexibility, and outstanding environmental stability. FPSCs. For the fabrication of high-quality perovskite films in FPSCs, many strategies, such as perovskite composition engineering, perovskite layer optimization, and additive and interface engineering can be used. Here we will discuss flexible perovskite solar cells with the highest efficiencies fabricated with different approaches. Spin-coated highest-efficiency flexible perovskite solar cells are produced with PCE of 25.83% with $FAPbI_3$ as an active layer [246]. By applying slot–die coating as an active-layer deposition technique for MAPbI3, 20.83% PCE is achieved [237]. For large, fabricated perovskite solar cells by spray coating technique, the highest PCE stands at 20.6% [247]. Screen-printed flexible perovskite devices were able to show a maximum of 15.89% efficiency [248]. With the help of the inkjet printing deposition approach, flexible perovskite showed the highest PCE of 21.65% for small-area cells [249]. Using the flexographic printing method to fabricate flexible solar cells, a maximum PCE of 15.3% is achieved [250]. Flexible perovskite made by blade-coating technique has shown the highest efficiency of 21.09% [251]. Gravure printing fabricated flexible PSCs showed a maximum of 19.1% efficiency [252]. Tables 4 and 5 are added for the generalized comparison of different fabrication approaches for substrate and active layers.

Tables 4 and 5 are based on the purely generalized comparison in which we have compared various techniques for the manufacturing of substrate layers, absorbing layers, charge-transport layers, and electrodes of the flexible solar devices. We have considered the following aspects of each technique: scalability, cost, precision, material waste, material usage, versatility, customization, adaptability, time of deposition, and dimensionality.

Table 4. Comparison of different deposition techniques of substrate layer for flexible solar cells.

Techniques	Scalability	Cost	Precision	Material Waste	Deposition Time	Dimensionality
Physical Vapor Deposition	Medium	Medium	Medium	Medium	Medium	3D
Spin Coating	Medium	Low	Medium	Medium	Medium	1D
Inkjet Printing	Medium	Medium	High	Medium	Low	2D
Spray Pyrolysis	High	Low	Low	High	Medium	2D
Chemical Vapor Deposition	High	High	High	Low	Low	3D
Sol–Gel Process	Low	Low	Medium	High	Medium	3D
Dip Coating	Medium	Low	Medium	Medium	Medium	1D
Roll-to-Roll Printing	High	Medium	Medium	Medium	High	1D
Electrospinning	Medium	Medium	High	Medium	Medium	3D
Molecular Beam Epitaxy	Low	High	High	Low	Low	0D

Note: The suitability levels (low, medium, high) for substrates, absorbing layer, charge-transport layers, and electrodes are generalized, and the actual applicability may vary based on specific manufacturing requirements and conditions.

Table 5. Comparison of different deposition techniques of absorbing layer for flexible solar cells.

Deposition Technique	Scalability	Cost	Precision	Material Waste	Deposition Time	Dimensionality
Spin Coating	Low	Low	Medium	Medium	Low	0D
Doctor Blade Coating	Medium	Medium	Medium	Medium	Medium	1D
Spray Coating	High	Low	Low	High	Medium	2D
Chemical Vapor Deposition	High	High	Low	High	Low	2D
Slot–Die Coating	High	Medium	High	Low	Medium	1D
Inkjet Printing	Medium	Medium	High	Medium	Low	2D
Atomic Layer Deposition	Low	High	High	Low	Low	0D
Screen Printing	Medium	Medium	Medium	Medium	Medium	2D
Sol–Gel Process	Low	Low	Medium	High	Medium	3D

Note: The suitability levels (low, medium, high) for substrates, absorbing layer, charge-transport layers, and electrodes are generalized, and the actual applicability may vary based on specific manufacturing requirements and conditions.

5. Commercialization

The flexible solar market has a promising future. Its current market size stands at 476 million USD and is expected to grow at a compound annual growth rate (CAGR) of 9.20%, reaching 1 billion USD by 2030 [4]. The commercialization of flexible solar is a crucial milestone in advancing and adapting new technologies in the PV industry. Over the last few decades, different photovoltaic technologies have emerged and transitioned from the laboratory to commercial applications. C-Si is the most abundant element in Earth's crust and has captured almost 95% of the PV market [255]. However, it has restricted flexibility due to the brittle nature and development of cracks under stresses, which limits its use for full-scale flexible PV modules. However, it is still one of the most attractive choices when it is used as a semi-flexible PV module [211]. At present, CdTe, Cu(Ind, Ga)(S, Se), and CIGS are the most common solar cells that exhibit flexibility. However, the PCE is lower, and the materials used are costly and toxic [256]. Similarly, perovskite solar cells, which have demonstrated rapid progress in stability and PCE in recent times, still face major bottlenecks in scaling up these technologies due to the unstable nature of the materials used in its development [257]. The successful capture of these technologies in flexible PV commercialization is increasing with more focus on its operational stability, manufacturing cost, and large-area fabrication of technologies.

Among different types of materials used for solar cells, Si has predominated, and to make it flexible, it has become more expensive and is still on the way to achieving its highest PCE [258]. CIGS solar cells have gained more attention in recent times due to their higher PCE than that of Si and, at the same time, provide flexibility and a good weight-to-power ratio [259]. CIGS is more stable as compared to perovskite, organic, and polymer-based solar cells. It is more environmentally friendly as compared to CdTe-based solar cells. However, it is expensive, and the availability of its constituent elements, such as indium and gallium, is a concern. GaAs-based solar cells are also facing a similar problem despite their higher PCE. Its application is more common in space due to its higher price. CZTS solar cells are cheaper because of their constituent elements, such as Zn and Sn. It is eco-friendly and highly stable. However, it has a lower PCE [260]. Table 6 below details the comparison of different solar cells based on different attributes.

Table 6. Comparison of different solar cells based on cost, fabrication temperature, PCE, and expected lifetime.

Type/Attribute	Cost ($/Kg) [261]	Fabrication Temperature	PCE	Expected Lifetime (Years)
c-Si	Si (500)	High (900)	26.81% [262]	20–25 [263]
CIGS	2200 (Ga) 600 (In) 140 (Se) 27 (Cu)	Low [264]	22.2% [265]	20 [266]
CdTe	240 (Te) 60 (Cd)	Low	22% [267]	20 [268]
CZTS	27 (Cu) 37 (Zn) 80 (Sn) 240 (S)	Medium [269]	12.6% [7]	10 [270]
GaAs	2200 (Ga) 3200 (As)	Low	29.1% [271]	10 [272]
Perovskite	1.5 (Cl) 4 (N) 15 (Pb) 24 (C) 49 (Br) 83 (I) 120 (H)	Low	25.7% [273]	Yet not commercialized due to stability issues
DSSC	200–300 (Dye Materials)	Low	13.5% [172]	6 [274,275]

6. Conclusions

This paper highlighted the recent progress and evolution in the materials used for flexible solar cells. Current progress in the literature on materials to improve the electrical, optical, and stability of different solar devices has been discussed. Silicon certainly dominates the current PV market; however, due to rapid technological development, the introduction of niche markets, newer applications, and the need for clean power, flexible PV technologies are growing rapidly. Comprehensive highlights of key materials used for flexible solar cells, such as active layers, electrodes, substrates, and fabrication techniques from the recent literature, are presented. c-Si has been widely used as active materials in semi-flexible PV due to the brittle nature of the silicon and lower PCE when made thinner. Light-management strategies have been investigated to improve its flexibility. In thin-film technologies, CIGS is dominating, with a-Si:H-based substrates also capturing the market soon. However, emerging solar-cell materials such as perovskite, organic solar cells, and quantum dots, due to their higher PCE and low cost of fabrication, are making their way toward commercialization. Transparent conductive oxides will continue to dominate as electrode materials with an increasing focus on conductive polymers. For substrate materials, polymers like PET, PEN, and PI are widely used in flexible PV; however, due to their lower OTR and WVTR, they need to be used in combination with a multilayer system with other polymers or need to be coated to improve the barrier properties.

Author Contributions: Conceptualization, M.M.; methodology, V.L.; formal analysis, V.L. and M.M.; investigation, M.M., V.L., Z.A. and S.A.B.S.; resources, data curation, M.M. and V.L.; writing—original draft preparation, M.M., V.L., Z.A. and S.A.B.S.; writing—review and editing, Z.A. and S.A.B.S.; visualization, Z.A.; supervision, V.L. All authors have read and agreed to the published version of the manuscript.

Funding: This research received no external funding.

Conflicts of Interest: The authors declare no conflicts of interest.

References

1. International Energy Agency. International Energy Agency (IEA) World Energy Outlook 2022. 2022; p. 524. Available online: https://www.iea.org/reports/world-energy-outlook-2022/executive-summary (accessed on 3 August 2023).
2. Roesch, R.; Faber, T.; von Hauff, E.; Brown, T.M.; Lira-Cantu, M.; Hoppe, H. Procedures and Practices for Evaluating Thin-Film Solar Cell Stability. *Adv. Energy Mater.* **2015**, *5*, 1501407. [CrossRef]
3. Reese, M.O.; Glynn, S.; Kempe, M.D.; McGott, D.L.; Dabney, M.S.; Barnes, T.M.; Booth, S.; Feldman, D.; Haegel, N.M. Increasing markets and decreasing package weight for high-specific-power photovoltaics. *Nat. Energy* **2018**, *3*, 1002–1012. [CrossRef]

4. Marpu, V.; Prakhar, J.E.P. Global Flexible Solar Panels Market. Technical Report. 2021. Available online: https://www.alliedmarketresearch.com/flexible-solar-panels-market-A14904 (accessed on 3 August 2023).
5. Song, N.; Deng, S. Thin Film Deposition Technologies and Application in Photovoltaics. In *Thin Films—Deposition Methods and Applications*; IntechOpen: London, UK, 2023. [CrossRef]
6. Yun, J. Ultrathin Metal films for Transparent Electrodes of Flexible Optoelectronic Devices. *Adv. Funct. Mater.* **2017**, *27*, 1606641. [CrossRef]
7. Park, J.S.; Kim, G.; Lee, S.; Lee, J.; Li, S.; Lee, J.; Kim, B.J. Material Design and Device Fabrication Strategies for Stretchable Organic Solar Cells. *Adv. Mater.* **2022**, *34*, 2201623. [CrossRef]
8. Li, J.; Dong, Q.; Li, N.; Wang, L. Direct Evidence of Ion Diffusion for the Silver-Electrode-Induced Thermal Degradation of Inverted Perovskite Solar Cells. *Adv. Energy Mater*. **2017**, *7*, 2922. [CrossRef]
9. Alajlani, Y.; Alaswad, A.; Placido, F.; Gibson, D.; Diyaf, A. Inorganic Thin Film Materials for Solar Cell Applications. In *Encyclopedia of Smart Materials*; Elsevier: Amsterdam, The Netherlands, 2018; pp. 386–399. [CrossRef]
10. Jung, H.S.; Han, G.S.; Park, N.G.; Ko, M.J. Flexible Perovskite Solar Cells. *Joule* **2019**, *3*, 1850–1880. [CrossRef]
11. Um, H.D.; Hwang, I.; Choi, D.; Seo, K. Flexible Crystalline-Silicon Photovoltaics: Light Management with Surface Structures. *Accounts Mater. Res.* **2021**, *2*, 701–713. [CrossRef]
12. Ramanujam, J.; Bishop, D.M.; Todorov, T.K.; Gunawan, O.; Rath, J.; Nekovei, R.; Artegiani, E.; Romeo, A. Flexible CIGS, CdTe and a-Si:H based thin film solar cells: A review. *Prog. Mater. Sci.* **2020**, *110*, 100619. [CrossRef]
13. Sharma, A.; Masoumi, S.; Gedefaw, D.; O'Shaughnessy, S.; Baran, D.; Pakdel, A. Flexible solar and thermal energy conversion devices: Organic photovoltaics (OPVs), organic thermoelectric generators (OTEGs) and hybrid PV-TEG systems. *Appl. Mater. Today* **2022**, *29*, 101614. [CrossRef]
14. Best Research-Cell Efficiency Chart—Nrel.gov. Available online: https://www.nrel.gov/pv/cell-efficiency.html (accessed on 17 June 2024).
15. Goje, A.; Ludin, N.; Fahsyar, P.; Syafiq, U.; Chelvanathan, P.; Syakirin, A.; Teridi, M.; Ibrahim, M.; Su'ait, M.; Sepeai, S.; et al. Review of flexible perovskite solar cells for indoor and outdoor applications. *Mater. Renew. Sustain. Energy* **2024**, *13*, 155–179. [CrossRef]
16. An, J.; Shen, Y.; Roca i Cabarrocas, P.; Chen, W. Fabrication of Crystalline Si Thin Films for Photovoltaics. *Phys. Status Solidi (RRL)—Rapid Res. Lett.* **2022**, *16*, 2200290. [CrossRef]
17. Li, L.; Han, L.; Hu, H.; Zhang, R. A review on polymers and their composites for flexible electronics. *Mater. Adv.* **2023**, *4*, 726–746. [CrossRef]
18. Ullah, H.; Czapp, S.; Szultka, S.; Tariq, H.; Qasim, U.B.; Imran, H. Crystalline Silicon (c-Si)-Based Tunnel Oxide Passivated Contact (TOPCon) Solar Cells: A Review. *Energies* **2023**, *16*, 715. [CrossRef]
19. Schneller, E.J.; Brooker, R.P.; Shiradkar, N.S.; Rodgers, M.P.; Dhere, N.G.; Davis, K.O.; Seigneur, H.P.; Mohajeri, N.; Wohlgemuth, J.; Scardera, G.; et al. Manufacturing metrology for c-Si module reliability and durability Part III: Module manufacturing. *Renew. Sustain. Energy Rev.* **2016**, *59*, 992–1016. [CrossRef]
20. Lee, T.D.; Ebong, A.U. A review of thin film solar cell technologies and challenges. *Renew. Sustain. Energy Rev.* **2017**, *70*, 1286–1297. [CrossRef]
21. Wang, S.; Weil, B.D.; Li, Y.; Wang, K.X.; Garnett, E.; Fan, S.; Cui, Y. Large-Area Free-Standing Ultrathin Single-Crystal Silicon as Processable Materials. *Nano Lett.* **2013**, *13*, 4393–4398. [CrossRef]
22. Hwang, I.; Um, H.D.; Kim, B.S.; Wober, M.; Seo, K. Flexible crystalline silicon radial junction photovoltaics with vertically aligned tapered microwires. *Energy Environ. Sci.* **2018**, *11*, 641–647. [CrossRef]
23. Kosten, E.D.; Warren, E.L.; Atwater, H.A. Ray optical light trapping in silicon microwires: Exceeding the 2n2 intensity limit. *Opt. Express* **2011**, *19*, 3316. [CrossRef] [PubMed]
24. Parise, M. On the electromagnetic field of an overhead line current source. *Electronics* **2020**, *9*, 2009. [CrossRef]
25. Leem, J.W.; Yu, J.S. Artificial inverted compound eye structured polymer films with light-harvesting and self-cleaning functions for encapsulated III–V solar cell applications. *RSC Adv.* **2015**, *5*, 60804–60813. [CrossRef]
26. Goetzberger, A. Optical confinement in thin Si-solar cells by diffuse back reflectors. In Proceedings of the 15th Photovoltaic Specialists Conference, Ann Arbor, MI, USA, 11–15 May 1981; pp. 867–870.
27. Meier, J.; Flückiger, R.; Keppner, H.; Shah, A. Complete microcrystalline p-i-n solar cell—Crystalline or amorphous cell behavior? *Appl. Phys. Lett.* **1994**, *65*, 860–862. [CrossRef]
28. Torres, P.; Meier, J.; Flückiger, R.; Kroll, U.; Selvan, J.A.A.; Keppner, H.; Shah, A.; Littelwood, S.D.; Kelly, I.E.; Giannoulès, P. Device grade microcrystalline silicon owing to reduced oxygen contamination. *Appl. Phys. Lett.* **1996**, *69*, 1373–1375. [CrossRef]
29. Mai, Y.; Klein, S.; Carius, R.; Stiebig, H.; Houben, L.; Geng, X.; Finger, F. Improvement of open circuit voltage in microcrystalline silicon solar cells using hot wire buffer layers. *J. Non-Cryst. Solids* **2006**, *352*, 1859–1862. [CrossRef]
30. Sai, H.; Matsui, T.; Matsubara, K.; Kondo, M.; Yoshida, I. 11.0%-Efficient Thin-Film Microcrystalline Silicon Solar Cells with Honeycomb Textured Substrates. *IEEE J. Photovoltaics* **2014**, *4*, 1349–1353. [CrossRef]

31. Romano, D.; Kovacevic-Badstubner, I.; Parise, M.; Grossner, U.; Ekman, J.; Antonini, G. Rigorous dc Solution of Partial Element Equivalent Circuit Models including Conductive, Dielectric, and Magnetic Materials. *IEEE Trans. Electromagn. Compat.* **2020**, *62*, 870–879. [CrossRef]
32. Xue, M.; Nazif, K.N.; Lyu, Z.; Jiang, J.; Lu, C.Y.; Lee, N.; Zang, K.; Chen, Y.; Zheng, T.; Kamins, T.I.; et al. Free-standing 2.7 μm thick ultrathin crystalline silicon solar cell with efficiency above 12.0%. *Nano Energy* **2020**, *70*, 104466. [CrossRef]
33. Parise, M.; Lombardi, L.; Ferranti, F.; Antonini, G. Magnetic Coupling between Coplanar Filamentary Coil Antennas with Uniform Current. *IEEE Trans. Electromagn. Compat.* **2020**, *62*, 622–626. [CrossRef]
34. Reuter, M.; Brendle, W.; Tobail, O.; Werner, J.H. 50μm thin solar cells with 17.0% efficiency. *Sol. Energy Mater. Sol. Cells* **2009**, *93*, 704–706. [CrossRef]
35. Dross, F.; O'Sullivan, B.; Debucquoy, M.; Bearda, T.; Govaerts, J.; Labie, R.; Loozen, X.; Granata, S.; El Daif, O.; Trompoukis, C.; et al. 18% Efficiency IBC Cell With Rear-Surface Processed on Quartz. *IEEE J. Photovoltaics* **2013**, *3*, 684–689. [CrossRef]
36. Yoon, J.; Baca, A.J.; Park, S.I.; Elvikis, P.; Geddes, J.B.; Li, L.; Kim, R.H.; Xiao, J.; Wang, S.; Kim, T.H.; et al. Ultrathin silicon solar microcells for semitransparent, mechanically flexible and microconcentrator module designs. *Nat. Mater.* **2008**, *7*, 907–915. [CrossRef]
37. Cruz-Campa, J.L.; Okandan, M.; Resnick, P.J.; Clews, P.; Pluym, T.; Grubbs, R.K.; Gupta, V.P.; Zubia, D.; Nielson, G.N. Microsystems enabled photovoltaics: 14.9% efficient 14μm thick crystalline silicon solar cell. *Sol. Energy Mater. Sol. Cells* **2011**, *95*, 551–558. [CrossRef]
38. Tang, Q.; Shen, H.; Yao, H.; Gao, K.; Jiang, Y.; Yang, W.; Liu, Y. Cu-assisted chemical etching of bulk c-Si: A rapid and novel method to obtain 45 μm ultrathin flexible c-Si solar cells with asymmetric front and back light trapping structures. *Sol. Energy* **2018**, *170*, 263–272. [CrossRef]
39. Parise, M.; Romano, D.; Antonini, G. Loop Impedance of Single-Turn Circular Coils Lying on Conducting Media. *IEEE Trans. Electromagn. Compat.* **2022**, *64*, 580–584. [CrossRef]
40. Saha, S.; Hilali, M.M.; Onyegam, E.U.; Sarkar, D.; Jawarani, D.; Rao, R.A.; Mathew, L.; Smith, R.S.; Xu, D.; Das, U.K.; et al. Single heterojunction solar cells on exfoliated flexible ∼25 μm thick mono-crystalline silicon substrates. *Appl. Phys. Lett.* **2013**, *102*, 163904. [CrossRef]
41. Gupta, S.; Navaraj, W.T.; Lorenzelli, L.; Dahiya, R. Ultra-thin chips for high-performance flexible electronics. *NPJ Flex. Electron.* **2018**, *2*, 8. [CrossRef]
42. Han, S.E.; Chen, G. Toward the Lambertian Limit of Light Trapping in Thin Nanostructured Silicon Solar Cells. *Nano Lett.* **2010**, *10*, 4692–4696. [CrossRef] [PubMed]
43. Saive, R. Light trapping in thin silicon solar cells: A review on fundamentals and technologies. *Prog. Photovoltaics Res. Appl.* **2021**, *29*, 1125–1137. [CrossRef]
44. Manzoor, S.; Filipič, M.; Onno, A.; Topič, M.; Holman, Z.C. Visualizing light trapping within textured silicon solar cells. *J. Appl. Phys.* **2020**, *127*, 063104. [CrossRef]
45. Branham, M.S.; Hsu, W.C.; Yerci, S.; Loomis, J.; Boriskina, S.V.; Hoard, B.R.; Han, S.E.; Ebong, A.; Chen, G. Empirical Comparison of Random and Periodic Surface Light-Trapping Structures for Ultrathin Silicon Photovoltaics. *Adv. Opt. Mater.* **2016**, *4*, 858–863. [CrossRef]
46. Parise, M. Evaluation of the flux linkage between equally sized circular loops placed on a layered soil. *Prog. Electromagn. Res. Lett.* **2020**, *89*, 127–132. [CrossRef]
47. Ali Shameli, M.; Yousefi, L. Light trapping in thin film crystalline silicon solar cells using Multi-Scale photonic topological insulators. *Opt. Laser Technol.* **2022**, *145*, 107457. [CrossRef]
48. Kodati, R.B.; Rao, P.N. A Review of Solar Cell Fundamentals and Technologies. *Adv. Sci. Lett.* **2020**, *26*, 260–271.
49. Gogoi, M.; Bhattarai, S.; Das, T. A simulation approach for optimization of optical absorption in amorphous silicon solar cell. *Mater. Today Proc.* **2023**, *73*, 604–607. [CrossRef]
50. Ushasree, P.M.; Bora, B. Silicon Solar Cells. In *Solar Energy Capture Materials*; The Royal Society of Chemistry: Cambridge, UK, 2019; pp. 1–55. [CrossRef]
51. Shariah, A.; Bataineh, M. Electrical and Structural Properties of Crystallized Amorphous Silicon Thin Films. *Silicon* **2023**, *15*, 2727–2735. [CrossRef]
52. Romano, D.; Angelo, L.D.; Kovacevic-Badstubner, I.; Grossner, U.; Parise, M.; Antonini, G. Efficient Partial Elements Computation for the Non-Orthogonal PEEC Method Including Conductive, Dielectrics, and Magnetic Materials. *IEEE Trans. Magn.* **2022**, *58*, 1–11. [CrossRef]
53. van Swaaij, R.; Klaver, A. Comparison of amorphous silicon solar cell performance following light and high-energy electron-beam induced degradation. *J. Non-Cryst. Solids* **2008**, *354*, 2464–2467. [CrossRef]
54. Kang, H. Crystalline Silicon vs. Amorphous Silicon: The Significance of Structural Differences in Photovoltaic Applications. *IOP Conf. Ser. Earth Environ. Sci.* **2021**, *726*, 012001. [CrossRef]

55. Parise, M. On the Voltage Response of Homogeneous Earth Models in Central Loop Electromagnetic Sounding. *Int. J. Antennas Propag.* **2022**, *2022*, 8294000. [CrossRef]
56. Rathore, N.; Panwar, N.L.; Yettou, F.; Gama, A. A comprehensive review of different types of solar photovoltaic cells and their applications. *Int. J. Ambient. Energy* **2021**, *42*, 1200–1217. [CrossRef]
57. Stuckelberger, M.; Biron, R.; Wyrsch, N.; Haug, F.J.; Ballif, C. Review: Progress in solar cells from hydrogenated amorphous silicon. *Renew. Sustain. Energy Rev.* **2017**, *76*, 1497–1523. [CrossRef]
58. Osayemwenre, G.O.; Meyer, E.L. Confirmation of the Degradation of Single Junction Amorphous Silicon Modules (a-Si:H). *Int. J. Photoenergy* **2019**, *2019*, 1–13. [CrossRef]
59. Hsu, C.; Lin, Y.; Hsu, H.; Tsai, C. Enhanced spectral response by silicon nitride index matching layer in amorphous silicon thin-film solar cells. *J. Non-Cryst. Solids* **2012**, *358*, 2324–2326. [CrossRef]
60. Oh, J.H.; Yang, J.H.; Lim, K.S.; Han, K.S.; Kim, Y.D.; Lee, H.; Song, J.H.; Kim, K.K.; Seong, T.Y. Effect of TiO_2 nanopatterns on the performance of hydrogenated amorphous silicon thin-film solar cells. *Thin Solid Film.* **2012**, *520*, 6287–6290. [CrossRef]
61. Takenezawa, J.; Hasumi, M.; Sameshima, T.; Koida, T.; Kaneko, T.; Karasawa, M.; Kondo, M. Heat treatment of amorphous silicon p-i-n solar cells with high-pressure H_2O vapor. *J. Non-Cryst. Solids* **2012**, *358*, 2285–2288. [CrossRef]
62. Nunomura, S.; Sakata, I.; Matsubara, K. Impact of band tail distribution on carrier trapping in hydrogenated amorphous silicon for solar cell applications. *J. Non-Cryst. Solids* **2016**, *436*, 44–50. [CrossRef]
63. Sharma, M.; Chaudhary, D.; Dwivedi, N.; Sudhakar, S.; Kumar, S. Simulating the Role of TCO Materials, their Surface Texturing and Band Gap of Amorphous Silicon Layers on the Efficiency of Amorphous Silicon Thin Film Solar Cells. *Silicon* **2017**, *9*, 59–68. [CrossRef]
64. Green, M.A.; Dunlop, E.D.; Siefer, G.; Yoshita, M.; Kopidakis, N.; Bothe, K.; Hao, X. Solar cell efficiency tables (Version 61). *Prog. Photovoltaics Res. Appl.* **2022**, *31*, 3–16. [CrossRef]
65. Hernádez-Mota, J.; Espíndola-Rodríguez, M.; Sánchez, Y.; López, I.; Peña, Y.; Saucedo, E. Thin film photovoltaic devices prepared with Cu_3BiS_3 ternary compound. *Mater. Sci. Semicond. Process.* **2018**, *87*, 37–43. [CrossRef]
66. Kim, S.; Quy, H.V.; Bark, C.W. Photovoltaic technologies for flexible solar cells: Beyond silicon. *Mater. Today Energy* **2021**, *19*, 100583. [CrossRef]
67. Xing, C.; Lei, Y.; Liu, M.; Wu, S.; He, W.; Zheng, Z. Environment-friendly Cu-based thin film solar cells: Materials, devices and charge carrier dynamics. *Phys. Chem. Chem. Phys.* **2021**, *23*, 16469–16487. [CrossRef] [PubMed]
68. Fischer, J.; Larsen, J.K.; Guillot, J.; Aida, Y.; Eisenbarth, T.; Regesch, D.; Depredurand, V.; Fevre, N.; Siebentritt, S.; Dale, P.J. Composition dependent characterization of copper indium diselenide thin film solar cells synthesized from electrodeposited binary selenide precursor stacks. *Sol. Energy Mater. Sol. Cells* **2014**, *126*, 88–95. [CrossRef]
69. Rühle, S. Tabulated values of the Shockley–Queisser limit for single junction solar cells. *Sol. Energy* **2016**, *130*, 139–147. [CrossRef]
70. Fukamizu, S.; Hironiwa, D.; Minemoto, T. Crystal quality improvement of $CuInS_2$ thin film by two step fabrication method with bismuth addition. *Appl. Mech. Mater.* **2013**, *372*, 563–566. [CrossRef]
71. Lim, Y.S.; Kwon, H.S.; Jeong, J.; Kim, J.Y.; Kim, H.; Ko, M.J.; Jeong, U.; Lee, D.K. Colloidal solution-processed CuInSe2 solar cells with significantly improved efficiency up to 9% by morphological improvement. *ACS Appl. Mater. Interfaces* **2014**, *6*, 259–267. [CrossRef]
72. Boubakeur, M.; Aissat, A.; Ben Arbia, M.; Maaref, H.; Vilcot, J. Enhancement of the efficiency of ultra-thin CIGS/Si structure for solar cell applications. *Superlattices Microstruct.* **2020**, *138*, 106377. [CrossRef]
73. Elhady, F.; M Abdolkader, T.; Fedawy, M. Simulation of new thin film Zn(O,S)/CIGS solar cell with bandgap grading. *Eng. Res. Express* **2023**, *5*, 025027. [CrossRef]
74. Nakamura, M.; Yamaguchi, K.; Kimoto, Y.; Yasaki, Y.; Kato, T.; Sugimoto, H. Cd-Free Cu(In,Ga)(Se,S) 2 Thin-Film Solar Cell with Record Efficiency of 23.35%. *IEEE J. Photovoltaics* **2019**, *9*, 1863–1867. [CrossRef]
75. Parise, M. Evaluation of the Inductive Coupling between Coplanar Concentric Coils in the Presence of the Ground. *Int. J. Antennas Propag.* **2024**, *2024*, 6640727. [CrossRef]
76. Rondiya, S.R.; Jadhav, Y.; Dzade, N.Y.; Ahammed, R.; Goswami, T.; De Sarkar, A.; Jadkar, S.; Haram, S.; Ghosh, H.N. Experimental and Theoretical Study into Interface Structure and Band Alignment of the $Cu_2Zn_{1-x}Cd_xSnS_4$ Heterointerface for Photovoltaic Applications. *ACS Appl. Energy Mater.* **2020**, *3*, 5153–5162. [CrossRef]
77. Sravani, L.; Routray, S.; Courel, M.; Pradhan, K. Loss mechanisms in CZTS and CZTSe Kesterite thin-film solar cells: Understanding the complexity of defect density. *Sol. Energy* **2021**, *227*, 56–66. [CrossRef]
78. Parise, M.; Loreto, F. Quasi-Static Explicit Expression for the Flux Linkage Between Noncoplanar Coils in Wireless Power Transfer Systems Above a Lossy Ground. *IEEE Trans. Electromagn. Compat.* **2023**, *65*, 1857–1867. [CrossRef]
79. Bosio, A.; Pasini, S.; Romeo, N. The History of Photovoltaics with Emphasis on CdTe Solar Cells and Modules. *Coatings* **2020**, *10*, 344. [CrossRef]
80. Wang, Y.; Wang, G.; Zhou, Y.; Xie, Q.; Chen, J.; Zheng, K.; Zheng, L.; Pan, J.; Wang, R. Research progress in doped absorber layer of CdTe solar cells. *Renew. Sustain. Energy Rev.* **2023**, *183*, 113427. [CrossRef]

81. Parise, M.; Loreto, F.; Romano, D.; Antonini, G.; Ekman, J. Accurate computation of mutual inductance of non coaxial pancake coils. *Energies* **2021**, *14*, 4907. [CrossRef]
82. Albin, D.S.; Amarasinghe, M.; Reese, M.O.; Moseley, J.; Moutinho, H.; Metzger, W.K. Colossal grain growth in Cd(Se,Te) thin films and their subsequent use in CdTe epitaxy by close-spaced sublimation. *J. Physics Energy* **2021**, *3*, 024003. [CrossRef]
83. Amarasinghe, M.; Sivananthan, S.; Metzger, W.K.; Colegrove, E.; Moutinho, H.; Albin, D.; Duenow, J.; Johnston, S.; Kephart, J.; Sampath, W.; et al. Influence of CdTe Deposition Temperature and Window Thickness on CdTe Grain Size and Lifetime After $CdCl_2$ Recrystallization. *IEEE J. Photovoltaics* **2018**, *8*, 600–603. [CrossRef]
84. Artegiani, E.; Major, J.D.; Shiel, H.; Dhanak, V.; Ferrari, C.; Romeo, A. How the amount of copper influences the formation and stability of defects in CdTe solar cells. *Sol. Energy Mater. Sol. Cells* **2020**, *204*, 110228. [CrossRef]
85. Bittau, F.; Artegiani, E.; Abbas, A.; Menossi, D.; Romeo, A.; Bowers, J.W.; Walls, J.M. Magnesium-doped Zinc Oxide as a High Resistance Transparent Layer for thin film CdS/CdTe solar cells. In Proceedings of the 2017 IEEE 44th Photovoltaic Specialist Conference (PVSC), Washington, DC, USA, 25–30 June 2017; pp. 752–756. [CrossRef]
86. Romeo, A.; Artegiani, E. CdTe-Based Thin Film Solar Cells: Past, Present and Future. *Energies* **2021**, *14*, 1684. [CrossRef]
87. Fiducia, T.A.M.; Mendis, B.G.; Li, K.; Grovenor, C.R.M.; Munshi, A.H.; Barth, K.; Sampath, W.S.; Wright, L.D.; Abbas, A.; Bowers, J.W.; et al. Understanding the role of selenium in defect passivation for highly efficient selenium-alloyed cadmium telluride solar cells. *Nat. Energy* **2019**, *4*, 504–511. [CrossRef]
88. Zheng, X.; Kuciauskas, D.; Moseley, J.; Colegrove, E.; Albin, D.S.; Moutinho, H.; Duenow, J.N.; Ablekim, T.; Harvey, S.P.; Ferguson, A.; et al. Recombination and bandgap engineering in CdSeTe/CdTe solar cells. *APL Mater.* **2019**, *7*, 071112. [CrossRef]
89. Metzger, W.K.; Grover, S.; Lu, D.; Colegrove, E.; Moseley, J.; Perkins, C.L.; Li, X.; Mallick, R.; Zhang, W.; Malik, R.; et al. Exceeding 20% efficiency with in situ group V doping in polycrystalline CdTe solar cells. *Nat. Energy* **2019**, *4*, 837–845. [CrossRef]
90. Nagaoka, A.; Nishioka, K.; Yoshino, K.; Katsube, R.; Nose, Y.; Masuda, T.; Scarpulla, M.A. Comparison of Sb, As, and P doping in Cd-rich CdTe single crystals: Doping properties, persistent photoconductivity, and long-term stability. *Appl. Phys. Lett.* **2020**, *116*, 132102. [CrossRef]
91. Parise, M.; Antonini, G.; Romano, D. On the Flux Linkage between Pancake Coils in Resonance-Type Wireless Power Transfer Systems. *Int. J. Antennas Propag.* **2020**, *2020*, 8630978. [CrossRef]
92. Xu, Z.; Zhuang, Q.; Zhou, Y.; Lu, S.; Wang, X.; Cai, W.; Zang, Z. Functional Layers of Inverted Flexible Perovskite Solar Cells and Effective Technologies for Device Commercialization. *Small Struct.* **2023**, *4*, 2200338. [CrossRef]
93. Parise, M.; Tamburrelli, V.; Antonini, G. Mutual impedance of thin-wire circular loops in near-surface applications. *IEEE Trans. Electromagn. Compat.* **2019**, *61*, 558–563. [CrossRef]
94. Quan, L.N.; Rand, B.P.; Friend, R.H.; Mhaisalkar, S.G.; Lee, T.W.; Sargent, E.H. Perovskites for Next-Generation Optical Sources. *Chem. Rev.* **2019**, *119*, 7444–7477. [CrossRef]
95. Kumar, M.H.; Yantara, N.; Dharani, S.; Graetzel, M.; Mhaisalkar, S.; Boix, P.P.; Mathews, N. Flexible, low-temperature, solution processed ZnO-based perovskite solid state solar cells. *Chem. Commun.* **2013**, *49*, 11089. [CrossRef]
96. Liu, D.; Kelly, T.L. Perovskite solar cells with a planar heterojunction structure prepared using room-temperature solution processing techniques. *Nat. Photonics* **2014**, *8*, 133–138. [CrossRef]
97. Feng, J.; Zhu, X.; Yang, Z.; Zhang, X.; Niu, J.; Wang, Z.; Zuo, S.; Priya, S.; Liu, S.F.; Yang, D. Record Efficiency Stable Flexible Perovskite Solar Cell Using Effective Additive Assistant Strategy. *Adv. Mater.* **2018**, *30*. [CrossRef] [PubMed]
98. Wu, C.; Wang, D.; Zhang, Y.; Gu, F.; Liu, G.; Zhu, N.; Luo, W.; Han, D.; Guo, X.; Qu, B.; et al. FAPbI 3 Flexible Solar Cells with a Record Efficiency of 19.38% Fabricated in Air via Ligand and Additive Synergetic Process. *Adv. Funct. Mater.* **2019**, *29*, 1902974. [CrossRef]
99. Yang, Y.; Min, F.; Qiao, Y.; Li, Z.; Vogelbacher, F.; Liu, Z.; Lv, W.; Wang, Y.; Song, Y. Embossed transparent electrodes assembled by bubble templates for efficient flexible perovskite solar cells. *Nano Energy* **2021**, *89*, 106384. [CrossRef]
100. Gao, D.; Li, B.; Li, Z.; Wu, X.; Zhang, S.; Zhao, D.; Jiang, X.; Zhang, C.; Wang, Y.; Li, Z.; et al. Highly Efficient Flexible Perovskite Solar Cells through Pentylammonium Acetate Modification with Certified Efficiency of 23.35%. *Adv. Mater.* **2023**, *35*, 2206387. [CrossRef]
101. Deepika.; Singh, A.; Verma, U.K.; Tonk, A. Device Structures of Perovskite Solar Cells: A Critical Review. *Phys. Status Solidi A* **2023**, *220*, 2200736. [CrossRef]
102. Parise, M.; Antonini, G.; Di Paola, L. A Rigorous Explicit Expression for the Mutual Inductance of Two Co-Axial Thin-Wire Coil Antennas Placed above a Layered Ground. *Energies* **2023**, *16*, 7586. [CrossRef]
103. Ha, J.; Kim, H.; Lee, H.; Lim, K.G.; Lee, T.W.; Yoo, S. Device architecture for efficient, low-hysteresis flexible perovskite solar cells: Replacing TiO_2 with C60 assisted by polyethylenimine ethoxylated interfacial layers. *Sol. Energy Mater. Sol. Cells* **2017**, *161*, 338–346. [CrossRef]
104. Gao, Y.; Huang, K.; Long, C.; Ding, Y.; Chang, J.; Zhang, D.; Etgar, L.; Liu, M.; Zhang, J.; Yang, J. Flexible Perovskite Solar Cells: From Materials and Device Architectures to Applications. *ACS Energy Lett.* **2022**, *7*, 1412–1445. [CrossRef]

105. Chung, J.; Shin, S.S.; Hwang, K.; Kim, G.; Kim, K.W.; Lee, D.S.; Kim, W.; Ma, B.S.; Kim, Y.K.; Kim, T.S.; et al. Record-efficiency flexible perovskite solar cell and module enabled by a porous-planar structure as an electron transport layer. *Energy Environ. Sci.* **2020**, *13*, 4854–4861. [CrossRef]
106. Ranjan, S.; Ranjan, R.; Tyagi, A.; Rana, K.S.; Soni, A.; Kodali, H.K.; Dalal, V.; Singh, A.; Garg, A.; Nalwa, K.S.; et al. Low-Temperature Microwave Processed TiO_2 as an Electron Transport Layer for Enhanced Performance and Atmospheric Stability in Planar Perovskite Solar Cells. *ACS Appl. Energy Mater.* **2022**, *5*, 2679–2696. [CrossRef]
107. Yang, D.; Yang, R.; Priya, S.; Liu, S.F. Recent Advances in Flexible Perovskite Solar Cells: Fabrication and Applications. *Angew. Chem. Int. Ed.* **2019**, *58*, 4466–4483. [CrossRef]
108. Targhi, F.F.; Jalili, Y.S.; Kanjouri, F. MAPbI3 and FAPbI3 perovskites as solar cells: Case study on structural, electrical and optical properties. *Results Phys.* **2018**, *10*, 616–627. [CrossRef]
109. Ono, L.K.; Juarez-Perez, E.J.; Qi, Y. Progress on Perovskite Materials and Solar Cells with Mixed Cations and Halide Anions. *ACS Appl. Mater. Interfaces* **2017**, *9*, 30197–30246. [CrossRef] [PubMed]
110. Pavlovetc, I.M.; Ruth, A.; Gushchina, I.; Ngo, L.; Zhang, S.; Zhang, Z.; Kuno, M. Distinguishing Models for Mixed Halide Lead Perovskite Photosegregation via Terminal Halide Stoichiometry. *ACS Energy Lett.* **2021**, *6*, 2064–2071. [CrossRef]
111. Lin, Q.; Kubicki, D.J.; Omrani, M.; Alam, F.; Abdi-Jalebi, M. The race between complicated multiple cation/anion compositions and stabilization of FAPbI 3 for halide perovskite solar cells. *J. Mater. Chem. C* **2023**, *11*, 2449–2468. [CrossRef]
112. Ye, F.; Yang, W.; Luo, D.; Zhu, R.; Gong, Q. Applications of cesium in the perovskite solar cells. *J. Semicond.* **2017**, *38*, 011003. [CrossRef]
113. Cao, B.; Yang, L.; Jiang, S.; Lin, H.; Wang, N.; Li, X. Flexible quintuple cation perovskite solar cells with high efficiency. *J. Mater. Chem. A* **2019**, *7*, 4960–4970. [CrossRef]
114. Kim, B.J.; Kim, D.H.; Lee, Y.Y.; Shin, H.W.; Han, G.S.; Hong, J.S.; Mahmood, K.; Ahn, T.K.; Joo, Y.C.; Hong, K.S.; et al. Highly efficient and bending durable perovskite solar cells: Toward a wearable power source. *Energy Environ. Sci.* **2015**, *8*, 916–921. [CrossRef]
115. Wu, S.; Li, Z.; Zhang, J.; Wu, X.; Deng, X.; Liu, Y.; Zhou, J.; Zhi, C.; Yu, X.; Choy, W.C.H.; et al. Low-Bandgap Organic Bulk-Heterojunction Enabled Efficient and Flexible Perovskite Solar Cells. *Adv. Mater.* **2021**, *33*, 2105539. [CrossRef] [PubMed]
116. Du, D.; Qiao, F.; Guo, Y.; Wang, F.; Wang, L.; Gao, C.; Zhang, D.; Liang, J.; Xu, Z.; Shen, W.; et al. Photovoltaic performance of flexible perovskite solar cells under bending state. *Sol. Energy* **2022**, *245*, 146–152. [CrossRef]
117. Du, D.; Zeng, Y.; Wang, C.; Li, M.; Wang, F.; Xu, Z.; Wang, H. Broadband antireflection enhancement of c-Si solar cells by less 1/10 wavelength and subwavelength of silica nanosphere coatings. *Opt. Mater.* **2021**, *114*, 110957. [CrossRef]
118. Meng, X.; Xing, Z.; Hu, X.; Chen, Y. Large-area Flexible Organic Solar Cells: Printing Technologies and Modular Design. *Chin. J. Polym. Sci.* **2022**, *40*, 1522–1566. [CrossRef]
119. Hosseinnezhad, M.; Ranjbar, Z. A review on flexible dye-sensitized solar cells as new sustainable energy resources. *Pigment. Resin Technol.* **2023**, *52*, 310–320. [CrossRef]
120. Cheng, P.; Li, G.; Zhan, X.; Yang, Y. Next-generation organic photovoltaics based on non-fullerene acceptors. *Nat. Photonics* **2018**, *12*, 131–142. [CrossRef]
121. Risi, B.G.; Riganti-Fulginei, F.; Laudani, A.; Quercio, M. Compensation Admittance Load Flow: A Computational Tool for the Sustainability of the Electrical Grid. *Sustainability* **2023**, *15*, 14427. [CrossRef]
122. Lin, Y.; Wang, J.; Zhang, Z.G.; Bai, H.; Li, Y.; Zhu, D.; Zhan, X. An Electron Acceptor Challenging Fullerenes for Efficient Polymer Solar Cells. *Adv. Mater.* **2015**, *27*, 1170–1174. [CrossRef] [PubMed]
123. Zhu, L.; Zhang, M.; Xu, J.; Li, C.; Yan, J.; Zhou, G.; Zhong, W.; Hao, T.; Song, J.; Xue, X.; et al. Single-junction organic solar cells with over 19% efficiency enabled by a refined double-fibril network morphology. *Nat. Mater.* **2022**, *21*, 656–663. [CrossRef]
124. Wei, Y.; Chen, Z.; Lu, G.; Yu, N.; Li, C.; Gao, J.; Gu, X.; Hao, X.; Lu, G.; Tang, Z.; et al. Binary Organic Solar Cells Breaking 19% via Manipulating the Vertical Component Distribution. *Adv. Mater.* **2022**, *34*, 2204718. [CrossRef]
125. Laudani, A.; Corti, F.; Intravaia, M.; Lozito, G.M.; Quercio, M.; Fulginei, F.R. Monitoring of BIPV by Means of a Low Cost Wireless Sensor Network. In Proceedings of the 2024 IEEE International Conference on Environment and Electrical Engineering and 2024 IEEE Industrial and Commercial Power Systems Europe (EEEIC / I&CPS Europe), Rome, Italy, 18–21 June 2024; pp. 1–5.
126. Li, M.; Igbari, F.; Wang, Z.; Liao, L. Indoor Thin-Film Photovoltaics: Progress and Challenges. *Adv. Energy Mater.* **2020**, *10*, 2000641. [CrossRef]
127. Zhang, S.; Chen, H.; Wang, P.; Li, S.; Li, Z.; Huang, Y.; Liu, J.; Yao, Z.; Li, C.; Wan, X.; et al. A Large Area Organic Solar Module with Non-Halogen Solvent Treatment, High Efficiency, and Decent Stability. *Sol. RRL* **2023**, *7*, 29. [CrossRef]
128. Quercio, M.; Galbusera, F.; Poskovic, E.; Franchini, F.; Ferraris, L.; Canova, A.; Gruosso, G.; Demir, A.G.; Previtali, B. Characterization of LPBF Produced Fe2.9wt.%Si for Electromagnetic Actuator. *IEEE Access* **2023**, *11*, 134822–134833. [CrossRef]
129. Liu, X.; Abernathy, M.R.; Metcalf, T.H.; Jugdersuren, B.; Culbertson, J.C.; Molina-Ruiz, M.; Hellman, F. Comparing amorphous silicon prepared by electron-beam evaporation and sputtering toward eliminating atomic tunneling states. *J. Alloys Compd.* **2021**, *855*, 157431. [CrossRef]

130. Fan, J.; Liu, Z.; Rao, J.; Yan, K.; Chen, Z.; Ran, Y.; Yan, B.; Yao, J.; Lu, G.; Zhu, H.; et al. High-Performance Organic Solar Modules via Bilayer-Merged-Annealing Assisted Blade Coating. *Adv. Mater.* **2022**, *34*, 2110569. [CrossRef]
131. Asghar, R.; Fulginei, F.R.; Quercio, M.; Maoz, M.; Sabino, L.; Abusara, M. Day-Ahead Photovoltaic Power Forecasting Using a Hybrid BiLSTM-CNN Model. In Proceedings of the 2024 Sixth International Conference on Intelligent Computing in Data Sciences (ICDS), Marrakech, Morocco, 23–24 October 2024; pp. 1–8.
132. Zhao, H.; Naveed, H.B.; Lin, B.; Zhou, X.; Yuan, J.; Zhou, K.; Wu, H.; Guo, R.; Scheel, M.A.; Chumakov, A.; et al. Hot Hydrocarbon-Solvent Slot-Die Coating Enables High-Efficiency Organic Solar Cells with Temperature-Dependent Aggregation Behavior. *Adv. Mater.* **2020**, *32*, 2002302. [CrossRef]
133. Zhao, H.; Lin, B.; Xue, J.; Naveed, H.B.; Zhao, C.; Zhou, X.; Zhou, K.; Wu, H.; Cai, Y.; Yun, D.; et al. Kinetics Manipulation Enables High-Performance Thick Ternary Organic Solar Cells via R2R-Compatible Slot-Die Coating. *Adv. Mater.* **2022**, *34*, 2105114. [CrossRef] [PubMed]
134. Ma, L.; Zhang, S.; Yao, H.; Xu, Y.; Wang, J.; Zu, Y.; Hou, J. High-Efficiency Nonfullerene Organic Solar Cells Enabled by 1000 nm Thick Active Layers with a Low Trap-State Density. *ACS Appl. Mater. Interfaces* **2020**, *12*, 18777–18784. [CrossRef]
135. Cai, Y.; Li, Y.; Wang, R.; Wu, H.; Chen, Z.; Zhang, J.; Ma, Z.; Hao, X.; Zhao, Y.; Zhang, C.; et al. A Well-Mixed Phase Formed by Two Compatible Non-Fullerene Acceptors Enables Ternary Organic Solar Cells with Efficiency over 18.6%. *Adv. Mater.* **2021**, *33*, 2101733. [CrossRef] [PubMed]
136. Yue, W.; Larsen-Olsen, T.T.; Hu, X.; Shi, M.; Chen, H.; Hinge, M.; Fojan, P.; Krebs, F.C.; Yu, D. Synthesis and photovoltaic properties from inverted geometry cells and roll-to-roll coated large area cells from dithienopyrrole-based donor—Acceptor polymers. *J. Mater. Chem. A* **2013**, *1*, 1785–1793. [CrossRef]
137. Qin, F.; Sun, L.; Chen, H.; Liu, Y.; Lu, X.; Wang, W.; Liu, T.; Dong, X.; Jiang, P.; Jiang, Y.; et al. 54 cm^2 Large-Area Flexible Organic Solar Modules with Efficiency Above 13%. *Adv. Mater.* **2021**, *33*, 2103017. [CrossRef] [PubMed]
138. Yan, T.; Song, W.; Huang, J.; Peng, R.; Huang, L.; Ge, Z. 16.67% Rigid and 14.06% Flexible Organic Solar Cells Enabled by Ternary Heterojunction Strategy. *Adv. Mater.* **2019**, *31*, 1902210. [CrossRef]
139. Song, W.; Yu, K.; Zhou, E.; Xie, L.; Hong, L.; Ge, J.; Zhang, J.; Zhang, X.; Peng, R.; Ge, Z. Crumple Durable Ultraflexible Organic Solar Cells with an Excellent Power-per-Weight Performance. *Adv. Funct. Mater.* **2021**, *31*, 2102694. [CrossRef]
140. Chen, Z.; Song, W.; Yu, K.; Ge, J.; Zhang, J.; Xie, L.; Peng, R.; Ge, Z. Small-molecular donor guest achieves rigid 18.5% and flexible 15.9% efficiency organic photovoltaic via fine-tuning microstructure morphology. *Joule* **2021**, *5*, 2395–2407. [CrossRef]
141. Wan, J.; Xia, Y.; Fang, J.; Zhang, Z.; Xu, B.; Wang, J.; Ai, L.; Song, W.; Hui, K.N.; Fan, X.; et al. Solution-Processed Transparent Conducting Electrodes for Flexible Organic Solar Cells with 16.61% Efficiency. *Nano-Micro Lett.* **2021**, *13*, 44. [CrossRef] [PubMed]
142. Zeng, G.; Chen, W.; Chen, X.; Hu, Y.; Chen, Y.; Zhang, B.; Chen, H.; Sun, W.; Shen, Y.; Li, Y.; et al. Realizing 17.5% Efficiency Flexible Organic Solar Cells via Atomic-Level Chemical Welding of Silver Nanowire Electrodes. *J. Am. Chem. Soc.* **2022**, *144*, 8658–8668. [CrossRef]
143. Ye, Q.; Chen, Z.; Yang, D.; Song, W.; Zhu, J.; Yang, S.; Ge, J.; Chen, F.; Ge, Z. Ductile Oligomeric Acceptor-Modified Flexible Organic Solar Cells Show Excellent Mechanical Robustness and Near 18% Efficiency. *Adv. Mater.* **2023**, *35*, 2305562. [CrossRef]
144. Röttger, A.; Boes, J.; Theisen, W.; Thiele, M.; Esen, C.; Edelmann, A.; Hellmann, R. Microstructure and mechanical properties of 316L austenitic stainless steel processed by different SLM devices. *Int. J. Adv. Manuf. Technol.* **2020**, *108*, 769–783. [CrossRef]
145. Quercio, M.; Galbusera, F.; Canova, A.; Demir, A.G.; Gruosso, G.; Previtali, B. Electromagnetic shielding properties of LPBF produced Fe2.9wt.%Si alloy. *J. Phys. Energy* **2023**, *5*, 045003. [CrossRef]
146. Meyland, M.J.; Nielsen, J.H.; Kocer, C. Tensile behaviour of soda-lime-silica glass and the significance of load duration—A literature review. *J. Build. Eng.* **2021**, *44*, 102966. [CrossRef]
147. Panowicz, R.; Konarzewski, M.; Durejko, T.; Szala, M.; Łazińska, M.; Czerwińska, M.; Prasuła, P. Properties of Polyethylene Terephthalate (PET) after Thermo-Oxidative Aging. *Materials* **2021**, *14*, 3833. [CrossRef] [PubMed]
148. Nakamura, N.; Mori, K.i.; Okada, H.; Abe, Y. Punching test for estimating tensile strength and total elongation of steel sheets. *Int. J. Adv. Manuf. Technol.* **2021**, *114*, 1847–1858. [CrossRef]
149. Subudhi, P.; Punetha, D. Progress, challenges, and perspectives on polymer substrates for emerging flexible solar cells: A holistic panoramic review. *Prog. Photovoltaics Res. Appl.* **2023**, *31*, 753–789. [CrossRef]
150. Kawano, Y.; Chantana, J.; Nishimura, T.; Mavlonov, A.; Minemoto, T. [Ga]/([Ga]+[In]) profile controlled through Ga flux for performance improvement of Cu(In,Ga)Se_2 solar cells on flexible stainless steel substrates. *J. Alloys Compd.* **2022**, *899*, 163276. [CrossRef]
151. Dai, X.; Deng, Y.; Van Brackle, C.H.; Chen, S.; Rudd, P.N.; Xiao, X.; Lin, Y.; Chen, B.; Huang, J. Scalable Fabrication of Efficient Perovskite Solar Modules on Flexible Glass Substrates. *Adv. Energy Mater.* **2020**, *10*, 1903108. [CrossRef]
152. Aghaei, M.; Fairbrother, A.; Gok, A.; Ahmad, S.; Kazim, S.; Lobato, K.; Oreski, G.; Reinders, A.; Schmitz, J.; Theelen, M.; et al. Review of degradation and failure phenomena in photovoltaic modules. *Renew. Sustain. Energy Rev.* **2022**, *159*, 112160. [CrossRef]
153. Aitola, K.; Gava Sonai, G.; Markkanen, M.; Jaqueline Kaschuk, J.; Hou, X.; Miettunen, K.; Lund, P.D. Encapsulation of commercial and emerging solar cells with focus on perovskite solar cells. *Sol. Energy* **2022**, *237*, 264–283. [CrossRef]

154. Madogni, V.I.; Kounouhéwa, B.; Akpo, A.; Agbomahéna, M.; Hounkpatin, S.A.; Awanou, C.N. Comparison of degradation mechanisms in organic photovoltaic devices upon exposure to a temperate and a subequatorial climate. *Chem. Phys. Lett.* **2015**, *640*, 201–214. [CrossRef]
155. Khodabandeh, F.; Golobostanfard, M.R. Flexible solar cells. In *Advanced Flexible Ceramics*; Elsevier: Amsterdam, The Netherlands, 2023; pp. 325–352. [CrossRef]
156. Castro-Hermosa, S.; Top, M.; Dagar, J.; Fahlteich, J.; Brown, T.M. Quantifying Performance of Permeation Barrier—Encapsulation Systems for Flexible and Glass-Based Electronics and Their Application to Perovskite Solar Cells. *Adv. Electron. Mater.* **2019**, *5*, 1800978. [CrossRef]
157. Huang, H.D.; Ren, P.G.; Zhong, G.J.; Olah, A.; Li, Z.M.; Baer, E.; Zhu, L. Promising strategies and new opportunities for high barrier polymer packaging films. *Prog. Polym. Sci.* **2023**, *144*, 101722. [CrossRef]
158. Amrutha, V.; Latha, S.; Bera, P.; John, S.; Srinivas, G.; Barshilia, H.C. Thermal treatment of stainless steel substrates along with a thin silicon layer for high temperature solar thermal applications. *Sol. Energy* **2023**, *262*, 111768. [CrossRef]
159. Canova, A.; Quercio, M. A Shielding System Proposal for the Cabling of Electric Glass Melters. *IEEE Open J. Ind. Appl.* **2023**, *4*, 1–10. [CrossRef]
160. Quercio, M.; del Pino Lopez, J.C.; Grasso, S.; Canova, A. Numerical and experimental analysis of thermal behaviour of high voltage power cable in unfilled ducts. *Sci. Rep.* **2024**, *14*, 20599. [CrossRef]
161. Nayshevsky, I.; Xu, Q.F.; Barahman, G.; Lyons, A.M. Fluoropolymer coatings for solar cover glass: Anti-soiling mechanisms in the presence of dew. *Sol. Energy Mater. Sol. Cells* **2020**, *206*, 110281. [CrossRef]
162. Yi, C.; Li, W.; Shi, S.; He, K.; Ma, P.; Chen, M.; Yang, C. High-temperature-resistant and colorless polyimide: Preparations, properties, and applications. *Sol. Energy* **2020**, *195*, 340–354. [CrossRef]
163. Lin, Q.; Huang, H.; Jing, Y.; Fu, H.; Chang, P.; Li, D.; Yao, Y.; Fan, Z. Flexible photovoltaic technologies. *J. Mater. Chem. C* **2014**, *2*, 1233. [CrossRef]
164. Feleki, B.T.; Bouwer, R.K.M.; Zardetto, V.; Wienk, M.M.; Janssen, R.A.J. p–i–n Perovskite Solar Cells on Steel Substrates. *ACS Appl. Energy Mater.* **2022**, *5*, 6709–6715. [CrossRef]
165. Heo, J.H.; Shin, D.H.; Lee, M.L.; Kang, M.G.; Im, S.H. Efficient Organic–Inorganic Hybrid Flexible Perovskite Solar Cells Prepared by Lamination of Polytriarylamine/$CH_3NH_3PbI_3$/Anodized Ti Metal Substrate and Graphene/PDMS Transparent Electrode Substrate. *ACS Appl. Mater. Interfaces* **2018**, *10*, 31413–31421. [CrossRef]
166. Hamtaei, S.; Brammertz, G.; Poortmans, J.; Vermang, B. A review on barrier layers used in flexible stainless-steel based CIGS photovoltaic devices. *NPJ Flex. Electron.* **2023**, *7*, 36. [CrossRef]
167. Corti, F.; Laudani, A.; Lozito, G.M.; Palermo, M.; Quercio, M.; Pattini, F.; Rampino, S. Dynamic Analysis of a Supercapacitor DC-Link in Photovoltaic Conversion Applications. *Energies* **2023**, *16*, 5864. [CrossRef]
168. Wijewardane, S.; Kazmerski, L.L. Inventions, innovations, and new technologies: Flexible and lightweight thin-film solar PV based on CIGS, CdTe, and a-Si:H. *Sol. Compass* **2023**, *7*, 100053. [CrossRef]
169. Josten, S.; Koehler, T.; Marlow, F. Dye-sensitized solar cells on stainless steel. *Sol. Energy* **2022**, *247*, 346–354. [CrossRef]
170. Yang, T.; Li, K.; Li, X.; Li, J.; Hou, J.; Fan, X.; Guo, H.; Wang, R.; Wu, J.; Deng, A.; et al. Toward lossless photovoltaic efficiency of Laser-shaped flexible Cu(In,Ga)Se_2 solar cells on stainless steel substrates. *Sol. Energy* **2023**, *255*, 12–25. [CrossRef]
171. Chantana, J.; Kawano, Y.; Mavlonov, A.; Minemoto, T. Cu(In,Ga)(S,Se) 2 Solar Cell with Zn(O,S,OH) x Buffer on Stainless Steel Utilizing $Zn_{1-x}Mg_xO$ and $Zn_{1-x}Mg_xO$:Al. *ACS Appl. Energy Mater.* **2022**, *5*, 14262–14270. [CrossRef]
172. Zhang, C.; Qi, T.; Wang, W.; Zhao, C.; Xu, S.; Ma, M.; Feng, Y.; Li, W.; Chen, M.; Yang, C.; et al. High efficiency CIGS solar cells on flexible stainless steel substrate with SiO_2 diffusion barrier layer. *Sol. Energy* **2021**, *230*, 1033–1039. [CrossRef]
173. Kumar, S.; Chouhan, A.S.; Agarwal, H.; Avasthi, S. Perovskite solar cell devices on flexible stainless-steel substrate. In Proceedings of the 2019 IEEE 46th Photovoltaic Specialists Conference (PVSC), Chicago, IL, USA, 16–21 June 2019; pp. 0477–0479. [CrossRef]
174. Kumar, S.; Kant, R.; Anadkat, N.; Mehta, M.; Pawar, V.; Avasthi, S. Sputtered NiOx as a Hole Transport Layer in n-i-p Perovskite Solar Cells Manufactured on Steel Substrate. In Proceedings of the 2022 IEEE International Conference on Emerging Electronics (ICEE), Bangalore, India, 11–14 December 2022; pp. 1–4. [CrossRef]
175. Fuad, A.; Fibriyanti, A.A.; Mufti, N.; Taufiq, A.; Maryam, S.; Hidayat, N. Growth of $CH_3NH_3PbI_3$ Perovskite on Stainless Steel Substrate Layered by ZnO Nanoparticles Using One-Step Spin Coating Route. *J. Phys. Conf. Ser.* **2018**, *1011*, 012011. [CrossRef]
176. Lee, M.; Ko, Y.; Min, B.K.; Jun, Y. Silver Nanowire Top Electrodes in Flexible Perovskite Solar Cells using Titanium Metal as Substrate. *ChemSusChem* **2016**, *9*, 31–35. [CrossRef]
177. Zardetto, V.; Brown, T.M.; Reale, A.; Di Carlo, A. Substrates for flexible electronics: A practical investigation on the electrical, film flexibility, optical, temperature, and solvent resistance properties. *J. Polym. Sci. Part B Polym. Phys.* **2011**, *49*, 638–648. [CrossRef]
178. Calabrò, E.; Matteocci, F.; Palma, A.L.; Vesce, L.; Taheri, B.; Carlini, L.; Pis, I.; Nappini, S.; Dagar, J.; Battocchio, C.; et al. Low temperature, solution-processed perovskite solar cells and modules with an aperture area efficiency of 11%. *Sol. Energy Mater. Sol. Cells* **2018**, *185*, 136–144. [CrossRef]

179. Hülsmann, P.; Wallner, G. Permeation of water vapour through polyethylene terephthalate (PET) films for back-sheets of photovoltaic modules. *Polym. Test.* **2017**, *58*, 153–158. [CrossRef]
180. Hornak, J.; Kadlec, P.; Kopřiva, J.; Polanský, R. Dielectric, structural and mechanical properties of thermally aged biaxially oriented polymeric substrates for flexible electronics. *Polym. Degrad. Stab.* **2022**, *199*, 109906. [CrossRef]
181. Asghar, R.; Fulginei, F.R.; Quercio, M.; Mahrouch, A. Artificial Neural Networks for Photovoltaic Power Forecasting: A Review of Five Promising Models. *IEEE Access* **2024**, *12*, 90461–90485. [CrossRef]
182. Skafi, Z.; Xu, J.; Mottaghitalab, V.; Mivehi, L.; Taheri, B.; Jafarzadeh, F.; Podapangi, S.K.; Altamura, D.; Guascito, M.R.; Barba, L.; et al. Highly Efficient Flexible Perovskite Solar Cells on Polyethylene Terephthalate Films via Dual Halide and Low-Dimensional Interface Engineering for Indoor Photovoltaics. *Sol. RRL* **2023**, *7*, 2300324. [CrossRef]
183. Bae, J.Y. Polycarbonate-Photovoltaic Module for Flexibility, Toughness, and High Temperature. *J. Electr. Eng. Technol.* **2023**, *18*, 1263–1271. [CrossRef]
184. Lu, Z.; Lou, Y.; Ma, P.; Zhu, K.; Cong, S.; Wang, C.; Su, X.; Zou, G. Highly Flexible and Transparent Polylactic Acid Composite Electrode for Perovskite Solar Cells. *Sol. RRL* **2020**, *4*, 2000320. [CrossRef]
185. Urbaniak, A.; Igalson, M.; Pianezzi, F.; Bücheler, S.; Chirilă, A.; Reinhard, P.; Tiwari, A. Effects of Na incorporation on electrical properties of Cu(In,Ga)Se_2-based photovoltaic devices on polyimide substrates. *Sol. Energy Mater. Sol. Cells* **2014**, *128*, 52–56. [CrossRef]
186. Macrelli, G.; Varshneya, A.K.; Mauro, J.C. Ultra-thin glass as a substrate for flexible photonics. *Opt. Mater.* **2020**, *106*, 109994. [CrossRef]
187. Gerthoffer, A.; Roux, F.; Emieux, F.; Faucherand, P.; Fournier, H.; Grenet, L.; Perraud, S. CIGS solar cells on flexible ultra-thin glass substrates: Characterization and bending test. *Thin Solid Film.* **2015**, *592*, 99–104. [CrossRef]
188. Bedjaoui, M.; Poulet, S. Direct Bonding and Debonding Approach of Ultrathin Glass Substrates for High Temperature Devices. In Proceedings of the Proceedings–Electronic Components and Technology Conference, Las Vegas, NE, USA, 1–4 June 2017; pp. 725–732. [CrossRef]
189. Lucaferri, V.; Quercio, M.; Laudani, A.; Fulginei, F.R. A Review on Battery Model-Based and Data-Driven Methods for Battery Management Systems. *Energies* **2023**, *16*, 7807. [CrossRef]
190. Dou, B.; Whitaker, J.B.; Bruening, K.; Moore, D.T.; Wheeler, L.M.; Ryter, J.; Breslin, N.J.; Berry, J.J.; Garner, S.M.; Barnes, F.S.; et al. Roll-to-Roll Printing of Perovskite Solar Cells. *ACS Energy Lett.* **2018**, *3*, 2558–2565. [CrossRef]
191. Seo, W.O.; Kim, D.; Kim, J. Flexible CdTe/CdS solar cells on thin glass substrates. *Opt. Express* **2015**, *23*, A316. [CrossRef]
192. Bista, S.S.; Li, D.B.; Rijal, S.; Neupane, S.; Awni, R.A.; Jiang, C.S.; Xiao, C.; Subedi, K.K.; Song, Z.; Phillips, A.B.; et al. Water-Assisted Lift-Off Process for Flexible CdTe Solar Cells. *ACS Appl. Energy Mater.* **2023**, *6*, 885–891. [CrossRef]
193. Teloeken, A.; Lamb, D.; Dunlop, T.; Irvine, S. Effect of bending test on the performance of CdTe solar cells on flexible ultra-thin glass produced by MOCVD. *Sol. Energy Mater. Sol. Cells* **2020**, *211*, 110552. [CrossRef]
194. Dou, B.; Miller, E.M.; Christians, J.A.; Sanehira, E.M.; Klein, T.R.; Barnes, F.S.; Shaheen, S.E.; Garner, S.M.; Ghosh, S.; Mallick, A.; et al. High-Performance Flexible Perovskite Solar Cells on Ultrathin Glass: Implications of the TCO. *J. Phys. Chem. Lett.* **2017**, *8*, 4960–4966. [CrossRef]
195. Asghar, R.; Fulginei, F.R.; Quercio, M.; Ahmad, M.; Abusara, M. Application of Deep Learning Algorithms for BIPV Power Forecasting in Italy. In Proceedings of the 2024 IEEE International Conference on Environment and Electrical Engineering and 2024 IEEE Industrial and Commercial Power Systems Europe (EEEIC/I&CPS Europe), Rome, Italy, 18–21 June 2024; pp. 1–6.
196. Jamarkattel, M.K.; Phillips, A.B.; Liyanage, G.K.; Alfadhili, F.K.; Bastola, E.; Plotnikov, V.V.; Compaan, A.D.; Ellingson, R.J.; Heben, M.J. Ultra-Thin and Lightweight CdS/CdTe Solar Cell Fabricated on Ceramic Substrate for Space Applications. In Proceedings of the 2022 IEEE 49th Photovoltaics Specialists Conference (PVSC), Philadelphia, PA, USA, 5–10 June 2022; pp. 0348–0350. [CrossRef]
197. Zhang, Y.M.; Jia, Z.J.; Zhao, Z.Y. Secondary phases in Cu_2ZnSnS_4 thin film solar cell: The role of interfaces. *Phys. B Condens. Matter* **2022**, *626*, 413539. [CrossRef]
198. Weerasinghe, H.C.; Dkhissi, Y.; Scully, A.D.; Caruso, R.A.; Cheng, Y.B. Encapsulation for improving the lifetime of flexible perovskite solar cells. *Nano Energy* **2015**, *18*, 118–125. [CrossRef]
199. Palermo, M.; Forconi, F.; Belloni, E.; Quercio, M.; Lozito, G.M.; Fulginei, F.R. Optimization of a feedforward neural network's architecture for an HVAC system problem. In Proceedings of the 2023 3rd International Conference on Electrical, Computer, Communications and Mechatronics Engineering (ICECCME), Tenerife, Spain, 19–21 July 2023; pp. 1–6.
200. Kim, J.G.; Na, S.I.; Kim, H.K. Flexible and transparent IWO films prepared by plasma arc ion plating for flexible perovskite solar cells. *AIP Adv.* **2018**, *8*, 105122. [CrossRef]
201. Taylor, M.P.; Readey, D.W.; Van Hest, M.F.; Teplin, C.W.; Alleman, J.L.; Dabney, M.S.; Gedvilas, L.M.; Keyes, B.M.; To, B.; Perkins, J.D.; et al. The remarkable thermal stability of amorphous In-Zn-O transparent conductors. *Adv. Funct. Mater.* **2008**, *18*, 3169–3178. [CrossRef]
202. Yang, L.; Li, Y.; Wang, L.; Pei, Y.; Wang, Z.; Zhang, Y.; Lin, H.; Li, X. Exfoliated Fluorographene Quantum Dots as Outstanding Passivants for Improved Flexible Perovskite Solar Cells. *ACS Appl. Mater. Interfaces* **2020**, *12*, 22992–23001. [CrossRef] [PubMed]

203. Cho, E.; Kim, Y.Y.; Ham, D.S.; Lee, J.H.; Park, J.S.; Seo, J.; Lee, S.J. Highly efficient and stable flexible perovskite solar cells enabled by using plasma-polymerized-fluorocarbon antireflection layer. *Nano Energy* **2021**, *82*, 105737. [CrossRef]
204. Datta, R.S.; Syed, N.; Zavabeti, A.; Jannat, A.; Mohiuddin, M.; Rokunuzzaman, M.; Yue Zhang, B.; Rahman, M.A.; Atkin, P.; Messalea, K.A.; et al. Flexible two-dimensional indium tin oxide fabricated using a liquid metal printing technique. *Nat. Electron.* **2020**, *3*, 51–58. [CrossRef]
205. Chen, X.; Xu, G.; Zeng, G.; Gu, H.; Chen, H.; Xu, H.; Yao, H.; Li, Y.; Hou, J.; Li, Y. Realizing Ultrahigh Mechanical Flexibility and >15% Efficiency of Flexible Organic Solar Cells via a "Welding" Flexible Transparent Electrode. *Adv. Mater.* **2020**, *32*, 1908478. [CrossRef]
206. Tam, K.C.; Kubis, P.; Maisch, P.; Brabec, C.J.; Egelhaaf, H. Fully printed organic solar modules with bottom and top silver nanowire electrodes. *Prog. Photovoltaics Res. Appl.* **2022**, *30*, 528–542. [CrossRef]
207. Han, J.; Yuan, S.; Liu, L.; Qiu, X.; Gong, H.; Yang, X.; Li, C.; Hao, Y.; Cao, B. Fully indium-free flexible Ag nanowires/ZnO:F composite transparent conductive electrodes with high haze. *J. Mater. Chem. A* **2015**, *3*, 5375–5384. [CrossRef]
208. Wang, J.; Chen, X.; Jiang, F.; Luo, Q.; Zhang, L.; Tan, M.; Xie, M.; Li, Y.; Zhou, Y.; Su, W.; et al. Electrochemical Corrosion of Ag Electrode in the Silver Grid Electrode-Based Flexible Perovskite Solar Cells and the Suppression Method. *Sol. RRL* **2018**, *2*, 118. [CrossRef]
209. Ha, H.; Cheong, J.Y.; Yun, T.G.; Hwang, B. Polymeric Protection for Silver Nanowire-Based Transparent Conductive Electrodes: Performance and Applications. *Inorganics* **2023**, *11*, 409. [CrossRef]
210. Lee, H.B.; Jin, W.Y.; Ovhal, M.M.; Kumar, N.; Kang, J.W. Flexible transparent conducting electrodes based on metal meshes for organic optoelectronic device applications: A review. *J. Mater. Chem. C* **2019**, *7*, 1087–1110. [CrossRef]
211. Liu, W.; Liu, Y.; Yang, Z.; Xu, C.; Li, X.; Huang, S.; Shi, J.; Du, J.; Han, A.; Yang, Y.; et al. Flexible solar cells based on foldable silicon wafers with blunted edges. *Nature* **2023**, *617*, 717–723. [CrossRef] [PubMed]
212. Ji, C.; Liu, D.; Zhang, C.; Jay Guo, L. Ultrathin-metal-film-based transparent electrodes with relative transmittance surpassing 100%. *Nat. Commun.* **2020**, *11*, 3367. [CrossRef] [PubMed]
213. Xu, M.; Feng, J.; Fan, Z.J.; Ou, X.L.; Zhang, Z.Y.; Wang, H.Y.; Sun, H.B. Flexible perovskite solar cells with ultrathin Au anode and vapour-deposited perovskite film. *Sol. Energy Mater. Sol. Cells* **2017**, *169*, 8–12. [CrossRef]
214. Domanski, K.; Correa-Baena, J.P.; Mine, N.; Nazeeruddin, M.K.; Abate, A.; Saliba, M.; Tress, W.; Hagfeldt, A.; Grätzel, M. Not All That Glitters Is Gold: Metal-Migration-Induced Degradation in Perovskite Solar Cells. *ACS Nano* **2016**, *10*, 6306–6314. [CrossRef] [PubMed]
215. Gagandeep.; Singh, M.; Kumar, R.; Singh, V. Investigating the impact of layer properties on the performance of p-graphene/CH3NH3PbI3/n-cSi solar cell using numerical modelling. *Superlattices Microstruct.* **2020**, *140*, 106468. [CrossRef]
216. Kaltenbrunner, M.; Adam, G.; Głowacki, E.D.; Drack, M.; Schwödiauer, R.; Leonat, L.; Apaydin, D.H.; Groiss, H.; Scharber, M.C.; White, M.S.; et al. Flexible high power-per-weight perovskite solar cells with chromium oxide–metal contacts for improved stability in air. *Nat. Mater.* **2015**, *14*, 1032–1039. [CrossRef]
217. Hu, X.; Huang, Z.; Zhou, X.; Li, P.; Wang, Y.; Huang, Z.; Su, M.; Ren, W.; Li, F.; Li, M.; et al. Wearable Large-Scale Perovskite Solar-Power Source via Nanocellular Scaffold. *Adv. Mater.* **2017**, *29*, 1703236. [CrossRef] [PubMed]
218. Zhang, Y.; Wu, Z.; Li, P.; Ono, L.K.; Qi, Y.; Zhou, J.; Shen, H.; Surya, C.; Zheng, Z. Fully Solution-Processed TCO-Free Semitransparent Perovskite Solar Cells for Tandem and Flexible Applications. *Adv. Energy Mater.* **2018**, *8*, 1701569. [CrossRef]
219. Vaagensmith, B.; Reza, K.M.; Hasan, M.N.; Elbohy, H.; Adhikari, N.; Dubey, A.; Kantack, N.; Gaml, E.; Qiao, Q. Environmentally Friendly Plasma-Treated PEDOT:PSS as Electrodes for ITO-Free Perovskite Solar Cells. *ACS Appl. Mater. Interfaces* **2017**, *9*, 35861–35870. [CrossRef] [PubMed]
220. Hu, X.; Meng, X.; Zhang, L.; Zhang, Y.; Cai, Z.; Huang, Z.; Su, M.; Wang, Y.; Li, M.; Li, F.; et al. A Mechanically Robust Conducting Polymer Network Electrode for Efficient Flexible Perovskite Solar Cells. *Joule* **2019**, *3*, 2205–2218. [CrossRef]
221. Hu, X.; Meng, X.; Yang, X.; Huang, Z.; Xing, Z.; Li, P.; Tan, L.; Su, M.; Li, F.; Chen, Y.; et al. Cementitious grain-boundary passivation for flexible perovskite solar cells with superior environmental stability and mechanical robustness. *Sci. Bull.* **2021**, *66*, 527–535. [CrossRef] [PubMed]
222. Fan, X.; Nie, W.; Tsai, H.; Wang, N.; Huang, H.; Cheng, Y.; Wen, R.; Ma, L.; Yan, F.; Xia, Y. PEDOT:PSS for Flexible and Stretchable Electronics: Modifications, Strategies, and Applications. Accepted *Adv. Sci.* **2019**, *6*, 1701569. [CrossRef] [PubMed]
223. Macdonald, T.J.; Batmunkh, M.; Lin, C.; Kim, J.; Tune, D.D.; Ambroz, F.; Li, X.; Xu, S.; Sol, C.; Papakonstantinou, I.; et al. Origin of Performance Enhancement in TiO_2-Carbon Nanotube Composite Perovskite Solar Cells. *Small Methods* **2019**, *3*, 1900164. [CrossRef]
224. Amini, A.; Abdizadeh, H.; Golobostanfard, M.R. Hybrid 1D/2D Carbon Nanostructure-Incorporated Titania Photoanodes for Perovskite Solar Cells. *ACS Appl. Energy Mater.* **2020**, *3*, 6195–6204. [CrossRef]
225. Tiong, V.T.; Pham, N.D.; Wang, T.; Zhu, T.; Zhao, X.; Zhang, Y.; Shen, Q.; Bell, J.; Hu, L.; Dai, S.; et al. Octadecylamine-Functionalized Single-Walled Carbon Nanotubes for Facilitating the Formation of a Monolithic Perovskite Layer and Stable Solar Cells. *Adv. Funct. Mater.* **2018**, *28*, 1705545. [CrossRef]

226. Lin, H.S.; Okawa, S.; Ma, Y.; Yotsumoto, S.; Lee, C.; Tan, S.; Manzhos, S.; Yoshizawa, M.; Chiashi, S.; Lee, H.M.; et al. Polyaromatic Nanotweezers on Semiconducting Carbon Nanotubes for the Growth and Interfacing of Lead Halide Perovskite Crystal Grains in Solar Cells. *Chem. Mater.* **2020**, *32*, 5125–5133. [CrossRef]
227. Seo, S.; Jeon, I.; Xiang, R.; Lee, C.; Zhang, H.; Tanaka, T.; Lee, J.W.; Suh, D.; Ogamoto, T.; Nishikubo, R.; et al. Semiconducting carbon nanotubes as crystal growth templates and grain bridges in perovskite solar cells. *J. Mater. Chem. A* **2019**, *7*, 12987–12992. [CrossRef]
228. Hatton, R.A.; Miller, A.J.; Silva, S.R.P. Carbon nanotubes: A multi-functional material for organic optoelectronics. *J. Mater. Chem.* **2008**, *18*, 1183. [CrossRef]
229. Jeon, I.; Chiba, T.; Delacou, C.; Guo, Y.; Kaskela, A.; Reynaud, O.; Kauppinen, E.I.; Maruyama, S.; Matsuo, Y. Single-Walled Carbon Nanotube Film as Electrode in Indium-Free Planar Heterojunction Perovskite Solar Cells: Investigation of Electron-Blocking Layers and Dopants. *Nano Lett.* **2015**, *15*, 6665–6671. [CrossRef]
230. Jeon, I.; Yoon, J.; Ahn, N.; Atwa, M.; Delacou, C.; Anisimov, A.; Kauppinen, E.I.; Choi, M.; Maruyama, S.; Matsuo, Y. Carbon Nanotubes versus Graphene as Flexible Transparent Electrodes in Inverted Perovskite Solar Cells. *J. Phys. Chem. Lett.* **2017**, *8*, 5395–5401. [CrossRef] [PubMed]
231. Jeon, I.; Yoon, J.; Kim, U.; Lee, C.; Xiang, R.; Shawky, A.; Xi, J.; Byeon, J.; Lee, H.M.; Choi, M.; et al. High-Performance Solution-Processed Double-Walled Carbon Nanotube Transparent Electrode for Perovskite Solar Cells. *Adv. Energy Mater.* **2019**, *9*, 1901204. [CrossRef]
232. Luo, Q.; Ma, H.; Hou, Q.; Li, Y.; Ren, J.; Dai, X.; Yao, Z.; Zhou, Y.; Xiang, L.; Du, H.; et al. All-Carbon-Electrode-Based Endurable Flexible Perovskite Solar Cells. *Adv. Funct. Mater.* **2018**, *28*, 1706777. [CrossRef]
233. Yoon, J.; Sung, H.; Lee, G.; Cho, W.; Ahn, N.; Jung, H.S.; Choi, M. Superflexible, high-efficiency perovskite solar cells utilizing graphene electrodes: Towards future foldable power sources. *Energy Environ. Sci.* **2017**, *10*, 337–345. [CrossRef]
234. Heo, J.H.; Shin, D.H.; Jang, M.H.; Lee, M.L.; Kang, M.G.; Im, S.H. Highly flexible, high-performance perovskite solar cells with adhesion promoted AuCl 3 -doped graphene electrodes. *J. Mater. Chem. A* **2017**, *5*, 21146–21152. [CrossRef]
235. Maniruzzaman, M.; Abdur, R.; Kuddus Sheikh, M.A.; Singh, S.; Lee, J. Conductive MoO3–PEDOT:PSS Composite Layer in MoO3/Au/MoO3–PEDOT:PSS Multilayer Electrode in ITO-Free Organic Solar Cells. *Processes* **2023**, *11*, 594. [CrossRef]
236. Xie, H.; Liang, T.; Yin, X.; Liu, J.; Liu, D.; Wang, G.; Gao, B.; Que, W. Mechanical Stability Study on PEDOT:PSS-Based ITO-Free Flexible Perovskite Solar Cells. *ACS Appl. Energy Mater.* **2022**, *5*, 3081–3091. [CrossRef]
237. Li, X.; Li, P.; Wu, Z.; Luo, D.; Yu, H.Y.; Lu, Z.H. Review and perspective of materials for flexible solar cells. *Mater. Rep. Energy* **2021**, *1*, 100001. [CrossRef]
238. Söderström, T.; Haug, F.J.; Terrazzoni-Daudrix, V.; Ballif, C. Optimization of amorphous silicon thin film solar cells for flexible photovoltaics. *J. Appl. Phys.* **2008**, *103*, 114509. [CrossRef]
239. Cao, S.; Yu, D.; Lin, Y.; Zhang, C.; Lu, L.; Yin, M.; Zhu, X.; Chen, X.; Li, D. Light Propagation in Flexible Thin-Film Amorphous Silicon Solar Cells with Nanotextured Metal Back Reflectors. *ACS Appl. Mater. Interfaces* **2020**, *12*, 26184–26192. [CrossRef] [PubMed]
240. Contreras, M.A.; Mansfield, L.M.; Egaas, B.; Li, J.; Romero, M.; Noufi, R.; Rudiger-Voigt, E.; Mannstadt, W. Wide bandgap Cu(In,Ga)Se_2 solar cells with improved energy conversion efficiency. *Prog. Photovoltaics Res. Appl.* **2012**, *20*, 843–850. [CrossRef]
241. Jackson, P.; Wuerz, R.; Hariskos, D.; Lotter, E.; Witte, W.; Powalla, M. Effects of heavy alkali elements in Cu(In,Ga)Se_2 solar cells with efficiencies up to 22.6%. *Phys. Status Solidi (RRL)—Rapid Res. Lett.* **2016**, *10*, 583–586. [CrossRef]
242. Chang, X.; Chen, J.; Ma, S.; Chen, B.; Zhang, X.; Gao, Q.; Li, F.; Wang, J.; Song, D.; Chen, J. Implementation of Tunneling Junction Passivated Contact Concept in Flexible CIGS Solar Cells. *Adv. Mater. Interfaces* **2023**, *10*, 2202171. [CrossRef]
243. Luo, J.; Tang, L.; Wang, S.; Yan, H.; Wang, W.; Chi, Z.; Gong, J.; Li, J.; Xiao, X. Manipulating Ga growth profile enables all-flexible high-performance single-junction CIGS and 4 T perovskite/CIGS tandem solar cells. *Chem. Eng. J.* **2023**, *455*, 140960. [CrossRef]
244. Carron, R.; Nishiwaki, S.; Feurer, T.; Hertwig, R.; Avancini, E.; Löckinger, J.; Yang, S.; Buecheler, S.; Tiwari, A.N. Advanced Alkali Treatments for High-Efficiency Cu(In,Ga)Se_2 Solar Cells on Flexible Substrates. *Adv. Energy Mater.* **2019**, *9*, 1900408. [CrossRef]
245. Pianezzi, F.; Chirilă, A.; Blösch, P.; Seyrling, S.; Buecheler, S.; Kranz, L.; Fella, C.; Tiwari, A.N. Electronic properties of Cu(In,Ga)Se_2 solar cells on stainless steel foils without diffusion barrier. *Prog. Photovoltaics Res. Appl.* **2012**, *20*, 253–259. [CrossRef]
246. Min, H.; Lee, D.Y.; Kim, J.; Kim, G.; Lee, K.S.; Kim, J.; Paik, M.J.; Kim, Y.K.; Kim, K.S.; Kim, M.G.; et al. Perovskite solar cells with atomically coherent interlayers on SnO2 electrodes. *Nature* **2021**, *598*, 444–450. [CrossRef]
247. Cai, H.; Liang, X.; Ye, X.; Su, J.; Guan, J.; Yang, J.; Liu, Y.; Zhou, X.; Han, R.; Ni, J.; et al. High Efficiency over 20% of Perovskite Solar Cells by Spray Coating via a Simple Process. *ACS Appl. Energy Mater.* **2020**, *3*, 9696–9702. [CrossRef]
248. Guan, Y.; Xu, M.; Zhang, W.; Li, D.; Hou, X.; Hong, L.; Wang, Q.; Zhang, Z.; Mei, A.; Chen, M.; et al. In situ transfer of $CH_3NH_3PbI_3$ single crystals in mesoporous scaffolds for efficient perovskite solar cells. *Chem. Sci.* **2020**, *11*, 474–481. [CrossRef]
249. Eggers, H.; Schackmar, F.; Abzieher, T.; Sun, Q.; Lemmer, U.; Vaynzof, Y.; Richards, B.S.; Hernandez-Sosa, G.; Paetzold, U.W. Inkjet-Printed Micrometer-Thick Perovskite Solar Cells with Large Columnar Grains. *Adv. Energy Mater.* **2020**, *10*, 1903184. [CrossRef]

250. Hösel, M.; Søndergaard, R.R.; Jørgensen, M.; Krebs, F.C. Comparison of UV-Curing, Hotmelt, and Pressure Sensitive Adhesive as Roll-to-R oll Encapsulation Methods for Polymer Solar Cells. *Adv. Eng. Mater.* **2013**, *15*, 1068–1075. [CrossRef]
251. Lee, K.M.; Chiu, W.H.; Tsai, Y.H.; Wang, C.S.; Tao, Y.T.; Lin, Y.D. High-performance perovskite solar cells based on dopant-free hole-transporting material fabricated by a thermal-assisted blade-coating method with efficiency exceeding 21%. *Chem. Eng. J.* **2022**, *427*, 131609. [CrossRef]
252. Kim, Y.Y.; Yang, T.Y.; Suhonen, R.; Kemppainen, A.; Hwang, K.; Jeon, N.J.; Seo, J. Roll-to-roll gravure-printed flexible perovskite solar cells using eco-friendly antisolvent bathing with wide processing window. *Nat. Commun.* **2020**, *11*, 5146. [CrossRef]
253. Tsao, C.S.; Chuang, C.M.; Cha, H.C.; Huang, Y.Y.; Sung, Y.M.; Chung, T.Y.; Chang, Y.T.; Hu, Z.C.; Liu, T.C.; Ma, W.Y.; et al. Lab-to-Fab development and long-term greenhouse test of stable flexible semitransparent organic photovoltaic module. *Mater. Today Energy* **2023**, *36*, 101340. [CrossRef]
254. Wang, Z.; Han, Y.; Yan, L.; Gong, C.; Kang, J.; Zhang, H.; Sun, X.; Zhang, L.; Lin, J.; Luo, Q.; et al. High Power Conversion Efficiency of 13.61% for 1 cm^2 Flexible Polymer Solar Cells Based on Patternable and Mass-Producible Gravure-Printed Silver Nanowire Electrodes. *Adv. Funct. Mater.* **2021**, *31*, 2007276. [CrossRef]
255. Philipps, S.; Ise, F.; Warmuth, W. Projects GmbH. In *Distribution of Cumulative Solar Photovoltaic Installations Worldwide as of 2021, by Region [Graph]*; Statista: Hamburg, Germany, 2023; p. 17.
256. Matsui, T.; Sai, H.; Bidiville, A.; Hsu, H.J.; Matsubara, K. Progress and limitations of thin-film silicon solar cells. *Sol. Energy* **2018**, *170*, 486–498. [CrossRef]
257. Chowdhury, T.A.; Bin Zafar, M.A.; Sajjad-Ul Islam, M.; Shahinuzzaman, M.; Islam, M.A.; Khandaker, M.U. Stability of perovskite solar cells: Issues and prospects. *RSC Adv.* **2023**, *13*, 1787–1810. [CrossRef] [PubMed]
258. Ballif, C.; Haug, F.J.; Boccard, M.; Verlinden, P.J.; Hahn, G. Status and perspectives of crystalline silicon photovoltaics in research and industry. *Nat. Rev. Mater.* **2022**, *7*, 597–616. [CrossRef]
259. Ishizuka, S.; Kamikawa, Y.; Nishinaga, J. Lightweight and flexible Cu(In,Ga)Se_2 solar minimodules: Toward 20% photovoltaic efficiency and beyond. *NPJ Flex. Electron.* **2022**, *6*, 90. [CrossRef]
260. Soonmin, H.; Hardani; Nandi, P.; Mwankemwa, B.S.; Malevu, T.D.; Malik, M.I. Overview on Different Types of Solar Cells: An Update. *Appl. Sci.* **2023**, *13*, 2051. [CrossRef]
261. Ardente, F.; Beylot, A.; Zampori, L. A price-based life cycle impact assessment method to quantify the reduced accessibility to mineral resources value. *Int. J. Life Cycle Assess.* **2023**, *28*, 95–109. [CrossRef]
262. At 26.81%, LONGi Sets a New World Record Efficiency for Silicon Solar Cells—LONGi—Longi.com. Available online: https://www.longi.com/en/news/propelling-the-transformation (accessed on 18 June 2024).
263. Libra, M.; Mrázek, D.; Tyukhov, I.; Severová, L.; Poulek, V.; Mach, J.; Šubrt, T.; Beránek, V.; Svoboda, R.; Sedláček, J. Reduced real lifetime of PV panels—Economic consequences. *Sol. Energy* **2023**, *259*, 229–234. [CrossRef]
264. Mufti, N.; Amrillah, T.; Taufiq, A.; Sunaryono; Aripriharta; Diantoro, M.; Zulhadjri; Nur, H. Review of CIGS-based solar cells manufacturing by structural engineering. *Sol. Energy* **2020**, *207*, 1146–1157. [CrossRef]
265. Swiss Scientists Achieve 22.2% Efficiency for Flexible CIGS Solar Cell. Available online: https://www.pv-magazine.com/2022/10/11/swiss-scientists-achieve-22-2-efficiency-for-flexible-cigs-solar-cell/ (accessed on 18 June 2024).
266. Amato, A.; Beolchini, F. End-of-life CIGS photovoltaic panel: A source of secondary indium and gallium. *Prog. Photovoltaics Res. Appl.* **2018**, *27*, 229–236. [CrossRef]
267. Scarpulla, M.A.; McCandless, B.; Phillips, A.B.; Yan, Y.; Heben, M.J.; Wolden, C.; Xiong, G.; Metzger, W.K.; Mao, D.; Krasikov, D.; et al. CdTe-based thin film photovoltaics: Recent advances, current challenges and future prospects. *Sol. Energy Mater. Sol. Cells* **2023**, *255*, 112289. [CrossRef]
268. Pastuszak, J.; Węgierek, P. Photovoltaic Cell Generations and Current Research Directions for Their Development. *Materials* **2022**, *15*, 5542. [CrossRef]
269. Nugroho, H.S.; Refantero, G.; Septiani, N.L.W.; Iqbal, M.; Marno, S.; Abdullah, H.; Prima, E.C.; Nugraha; Yuliarto, B. A progress review on the modification of CZTS(e)-based thin-film solar cells. *J. Ind. Eng. Chem.* **2022**, *105*, 83–110. [CrossRef]
270. Larramona, G.; Choné, C.; Meissner, D.; Ernits, K.; Bras, P.; Ren, Y.; Martín-Salinas, R.; Rodríguez-Villatoro, J.L.; Vermang, B.; Brammertz, G. Stability, reliability, upscaling and possible technological applications of kesterite solar cells. *J. Phys. Energy* **2020**, *2*, 024009. [CrossRef]
271. Yamaguchi, M. High-Efficiency GaAs-Based Solar Cells. In *Post-Transition Metals*; IntechOpen: London, UK, 2021. [CrossRef]
272. Wiesenfarth, M.; Steiner, M.; Dörsam, T.; Siefer, G.; Dimroth, F.; Nitz, P.; Bett, A.W. FLATCON® CPV module technology: A new design based on the evaluation of 10 years of outdoor measurement data. *AIP Conf. Proc.* **2019**, *2149*, 030007. [CrossRef]
273. Kim, H.; Lim, J.; Park, S.; Song, S. A review on the engineering of hole-transporting materials for perovskite solar cells with high efficiency and high stability. *Dye. Pigment.* **2023**, *218*, 111449. [CrossRef]

274. Zhang, S.; Lin, J.; Lin, R.; Radjenovic, P.; Yang, W.; Xu, J.; Dong, J.; Yang, Z.; Hang, W.; Tian, Z.; et al. In situ Raman study of the photoinduced behavior of dye molecules on TiO2(hkl) single crystal surfaces. *Chem. Sci.* **2020**, *11*, 6431–6435. [CrossRef]
275. Lombardi, L.; Loreto, F.; Ferranti, F.; Ruehli, A.; Nakhla, M.S.; Tao, Y.; Parise, M.; Antonini, G. Time-Domain Analysis of Retarded Partial Element Equivalent Circuit Models Using Numerical Inversion of Laplace Transform. *IEEE Trans. Electromagn. Compat.* **2021**, *63*, 870–879. [CrossRef]